THE USE OF REMOTELY SENSED LIDAR AND MULTISPECTRAL IMAGERY FOR MODELING EASTERN REDCEDAR BIOMASS WITHIN NORTH EASTERN KANSAS

By

JOHNNY BRYANT

B.S., Kansas State University, 2011

A THESIS

Submitted in partial fulfillment of the requirements for the degree

MASTER OF ARTS

Department of Geography
College of Arts and Sciences

KANSAS STATE UNIVERSITY
Manhattan, Kansas

2017

Approved by:

Major Professor
Kevin P. Price

Copyright

.

Abstract

Due in large part to changes in land management practices, eastern redcedar (Juniperus virginiana L.), a native Kansas conifer, is rapidly invading onto valuable rangelands. The suppression of fire and increase of intensive grazing, combined with the rapid growth rate, high reproductive output, and dispersal ability of the species have allowed it to dramatically expand beyond its original range. Based on its abundance and invasive nature there is a growing interest in harvesting this species for use as a biofuel. For economic planning purposes, density and biomass quantities for the trees are needed. Three methods are explored for mapping eastern redcedar and quantifying its biomass in Riley County, Kansas. First a comparison of plot-regression versus individual tree based techniques is conducted to determine the optimal approach for characterizing redcedar tree canopy using LiDAR (Light Detection and Ranging). Second a hybrid approach is utilized to characterize redcedar canopy biomass using LiDAR and high-resolution multispectral imagery. Finally, to explore alternative methods of characterizing the three-dimensional structure of redcedar canopy a comparison of "Structure from Motion" photogrammetric techniques and LiDAR is conducted. These methods showed promising results and proved to be useful in the forestry, range management, and bioenergy industries for better understanding the potential of invasive redcedar as a biofuel resource.

Table of Contents

List of Figures

List of Tables

Acknowledgements

I would like to acknowledge the Kansas State Forest service for funding this research and lending their time and equipment to help with the project.

I would also like to thank my committee, Drs. Kevin Price, Doug Goodin, and Deon van der Merwe for their support, mentoring, and patience throughout the process. My colleague David Burchfield collaborated with me on the third chapter and much of the field work and I would like to thank him for his contributions to the project. I would also like to thank Lynn Brien for her assistance in proofreading.

Lastly I would like to thank my wife and family without who's support and patience this process would not have been possible.

Chapter 1 - Characterizing the Invasion of Eastern Redcedar and Mapping its Biomass[1]

In recent decades, woody tree invasion has become a serious problem in the tallgrass prairie region of Eastern Kansas (Bragg & Hulbert, 1976). Due to rapid human settlement, overgrazing, and fire suppression, woody species have invaded sites that were once healthy tallgrass prairies (Briggs, *et al.*, 2002). Among the most invasive of these woody species is *Juniperus virginiana*, commonly known as eastern redcedar (Figure 1.1).

Figure 1-1 Eastern redcedar encroaching in a pasture near Russell, KS.

[1] Chapter Co-Authored with and Reprinted with Permission from David Burchfield

1.1 Species Description

Eastern redcedar (known hereafter as "redcedar") is the only juniper species native to the state of Kansas (Pease, 2007). It is a species characterized by its rapid growth and high reproductive output (Briggs, *et al.*, 2002). Redcedar is a coniferous species that has sharp, scaly leaves that perform photosynthesis (Stevens, *et al.*, 2005) (Figure 1.2). Unlike deciduous trees that lose their leaves during autumn, redcedar retains its leafy material throughout the year. Redcedar is a dioecious species—female redcedar can be identified by the presence of small, round, waxy blue seed cones (often called "berries") during certain times of the year (Van Haverbeke & Read, 1976; Stevens, *et al.*, 2005).

Figure 1-2 Eastern redcedar foliage.

The range of redcedar is extensive, spanning the eastern half of the United States from the Atlantic to the High Plains and from Texas in the south to Ontario in the north (Figure 1.3).

Isolated patches of redcedar have also been reported in Oregon. In Kansas, eastern redcedar grows primarily in the eastern two-thirds of the state where conditions are humid enough to support it (Stevens, *et al.*, 2005). It is also widely planted as a "backbone" windbreak species in Kansas (Strine, 2004). Due in part to these windbreak plantings across the state, the current range of redcedar exceeds its historical range (Owensby, *et al.*, 1973).

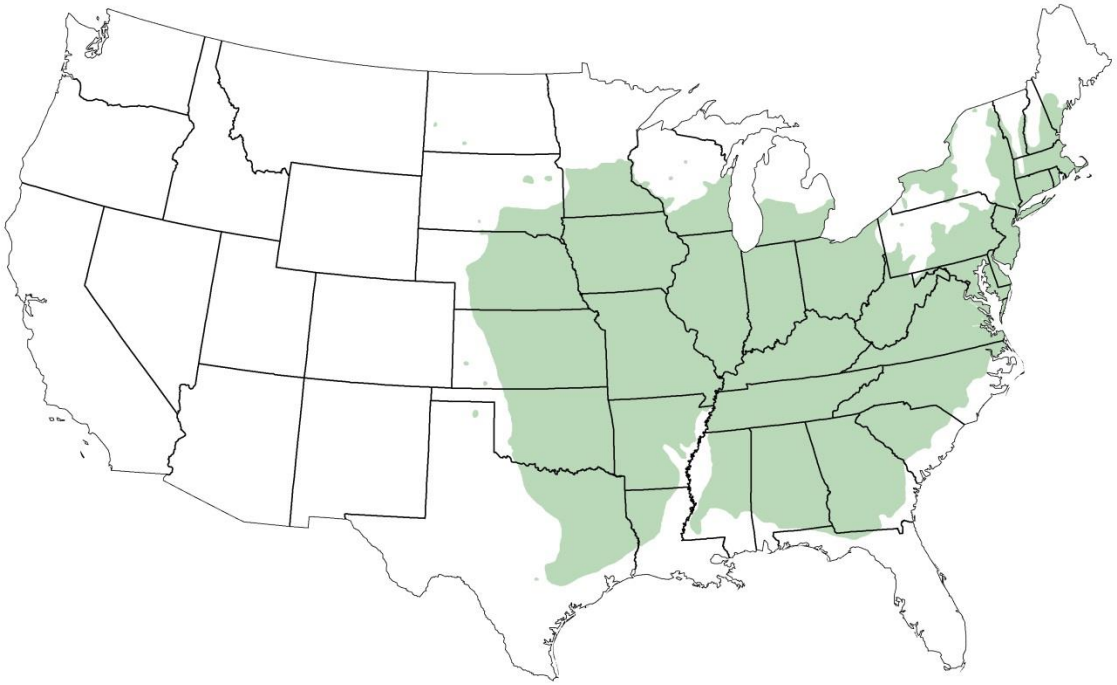

Figure 1-3 Range of eastern redcedar in the United States (derived from Little, 1971).

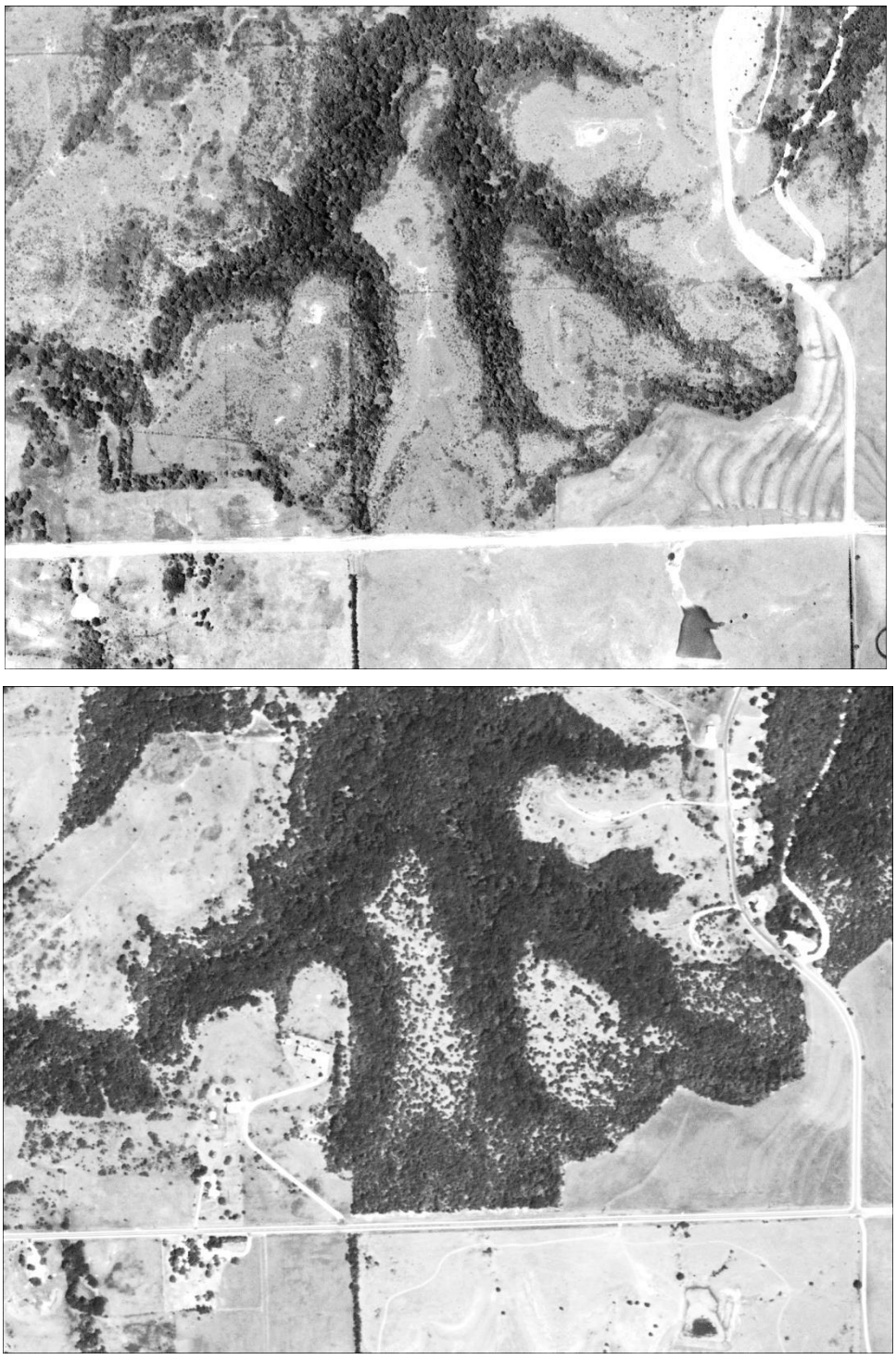

Figure 1-4 An example of redcedar (dark areas on the images) expansion in Riley County, KS, 1962 (top) to 2012 (bottom). (Images courtesy of USDA NAIP Program and KSU Historical Aerial Photo Archive)

1.2 Species Ecology and Human Factors

Eastern redcedar is a pioneer invader species that will readily spread over a short period (Van Haverbeke & Read, 1976). Prior to European settlement in Kansas, woody species (including redcedar) were primarily located in stream bottoms (lowlands) in the Flint Hills region (Bragg & Hulbert, 1976). The Spanish explorer Coronado wrote in 1541 as he travelled through the region, "There is not any kind of wood in all these plains, away from the gullies and rivers, which are very few" (Bragg & Hulbert, 1976). Before settlement occurred in the region, as woody species would spread into upland areas, they were naturally controlled by periodic wildfires. Dendrochronological dating methods have shown that, prior to European-American settlement, these fires burned in the Flint Hills every four years on average (Allen & Palmer, 2011). Within the historic range of redcedar European-American settlers fragmented the landscape, constructing artificial barriers to fire (primarily roads) that have halted the natural progression of prairie fires (Briggs, *et al.*, 2002). Poor land management and plantings of redcedar in windbreaks have further accelerated its spread (Owensby, *et al.*, 1973). These factors have caused redcedar to become established in upland tallgrass prairies.

Redcedar's invasiveness has become a problem in the Flint Hills region where many absentee landowners have acquired land as an investment or for hunting (Kindscher & Scott, 1997). These landowners may often be unwilling or unable to take the necessary steps—such as conducting annual prairie burns—to properly manage their property. As redcedar has spread into the uplands due to a lack of fire to control it, it has often turned into dense stands that crowd out warm-season (C_4) native tallgrass prairie grasses and forbs (Gehring & Bragg, 1992) (Figure 1.4). Many of these species are important forage plants for grazing animals in Kansas. Valuable rangelands can be converted into closed-canopy redcedar stands in as little as 40 years (Briggs, *et al.*, 2002). Beef cattle ranching, an important industry in Kansas representing $8.5 billion of the $13.4 billion agricultural industry in the state (USDA, 2011), is being threatened by the spread of redcedar into rangelands.

Another major concern with redcedar is its encroachment into populated areas. Redcedar foliage contains flammable volatile oils, and dense stands of redcedar located in urban and suburban areas can increase the risk of a wildfire affecting populated areas (Ward, 2013) (Figure 1.5) (Figure 1.6).

Figure 1-5 Eastern redcedar trees catching fire during a prairie burn. Image courtesy of the Kansas Forest Service.

Figure 1-6 Area of concern in Manhattan, KS, where a neighborhood borders a large redcedar stand (outlined in yellow). Redcedar stands encroaching in developed areas pose a high risk due to greater wildfire potential. Image courtesy of the USDA NAIP program.

1.3 Redcedar Uses

Eastern redcedar has been shown to be a useful species in industry and agriculture. It is commonly harvested for construction of pencils and wood chests, and it is also chipped into mulch for use in landscaping and gardening (Van Haverbeke & Read, 1976) (Figure 1.7). Redcedar oil has also been extracted for use in the essential oil industry (Gawde, *et al.*, 2009; CAFNR news, 2008; Semen & Hiziroglu, 2005). It has also been shown to contain a high amount of energy for heating. Large individual trees have been shown to contain over twelve million British Thermal Units (BTUs) of energy, equivalent to around 106 gallons of heating oil, or 0.6 tons of anthracite coal (Strauss, *et al.*, 2011; Slusher, 1995). One proposal is to harvest redcedar for use as a biofuel, providing an inexpensive, locally-obtained fuel source for Kansas.

Redcedar wood can be converted into biodiesel, wood chips for wood burning boilers, or "biochar," a charcoal soil amendment (Teel, 2012; Starks, *et al.*, 2011).

Figure 1-7 Eastern redcedar logs and mulch processed for gardening use near Pratt, Kansas. Image courtesy of Larry Biles.

1.4 Mapping of Redcedar Using Remotely Sensed Data

To facilitate economic planning and the development of an eastern redcedar biofuel industry in Kansas, redcedar cover and biomass estimates are needed on a detailed level. The purpose of this thesis is to explore methodologies and address questions regarding the use of remotely sensed data for measuring redcedar biomass and cover.

The initial objective of this thesis is to identify the best method for assessing redcedar biomass using Light Detection and Ranging (LiDAR). A second objective is to classify redcedar cover on the landscape using high spatial resolution (1-meter) National Agriculture Imagery Program (NAIP) imagery to identify redcedar canopy within a heterogonous canopy height model derived from LiDAR. A third objective is to map redcedar biomass across a large area (*e.g.* a county) using a fusion of satellite imagery, LiDAR data, and high spatial resolution color-infrared aerial photography. The fourth and final objective is to explore advances in structure

from motion photogrammetry (SfM) and how these advances may provide an alternative to LiDAR for 3D modeling of redcedar.

In chapter two I will explore two methods of characterizing the height and canopy of redcedar using LiDAR and evaluate these two methods for feasibility and accuracy. Chapter two and three will also include discussion on the methods applied to identify redcedar in a heterogeneous canopy height model by applying a mask derived from classified aerial imagery. In chapter three I will apply what is learned in chapter 2 to extract canopy metrics from the redcedar height model and use those to produce a predictive model to map redcedar biomass. I will also evaluate the accuracy and limitations to the biomass model. In Chapter four I will explore how a structure from motion derived surface model compares to data derived from LiDAR and how this newer technology might be applied for mapping redcedar canopy.

References

1. Anderson, J. R., E. E. Hardy, J. T. Roach, and R. E. Witmer. 1976. *A Land Use and Land Cover Classification System for Use with Remote Sensor Data*. Washington, D.C.: United States Government Printing Office.

2. Briggs, J. M., and D.J. Gibson. 1992. "Effect of Burning on Tree Spatial Patterns in a Tallgrass Prairie Landscape." *Bulletin of the Torrey Botanical Club* 119: 300–307.

3. Briggs, J. M., G. A. Hoch, and L. C. Johnson. 2002. "Assessing the Rate, Mechanisms, and Consequences of the Conversion of Tallgrass Prairie to Juniperus Virginiana Forest." *Ecosystems*. 5 (6): 578–586.

4. Briggs, J. M., A. K. Knapp, and B. L. Brock. 2002. "Expansion of Woody Plants in Tallgrass Prairie: A Fifteen-Year Study of Fire and Fire-Grazing Interactions." *American Midland Naturalist* 147 (2): 287–294.
URL: http://www.jstor.org/stable/3083203.

5. Coppedge, B. R., D. M. Engle, R. E. Masters, and M. S. Gregory. (2001). "Avian Response to Landscape Change in Fragmented Southern Great Plains Grasslands." *Ecological Applications* 11 (1): 47–59.

6. Chapman, R. N., D. M. Engle, R. E. Masters, and D. M. Leslie Jr. (2004) "Tree Invasion Constrains the Influence of Herbaceous Structure in Grassland Bird Habitats." *Ecoscience* 11 (1): 56–63.

7. Drake, J. B., R. G. Knox, R. O. Dubayah, D. B. Clark, R. Condit, J. B. Blair, And M. Hofton. (2003). "Above-Ground Biomass Estimation in Closed Canopy Neotropical Forests Using Lidar Remote Sensing: Factors Affecting the Generality of Relationships." *Global Ecology and Biogeography* 12 (2): 147–159.

8. Horncastle, V. J., E. C. Hellgren, P. M. Mayer, A. C. Ganguli, D. M. Engle, And D. M. Leslie Jr. (2005) "Implications of Invasion by Juniperus Virginiana on Small Mammals in The Southern Great Plains." *Journal of Mammalogy* 86 (6): 1144–1155.

9. Jensen, J. R. 2005. *Introductory Digital Image Processing: A Remote Sensing Perspective*. Upper Saddle River: Pearson Prentice Hall.

10. Lucas, R. M., N. Cronin, A. Lee, M. Moghaddam, C. Witte, and P. Tickle. (2006). "Empirical Relationships between AIRSAR Backscatter and Lidar-Derived Forest Biomass, Queensland, Australia." *Remote Sensing of Environment* 100 (3):407–425.

11. Norris, M., J. Blair, L. Johnson, and R. Mckane. (2001). "Assessing Changes in Biomass, Productivity, and C and N Stores Following Juniperus Virginiana Forest Expansion into

Tallgrass Prairie" Canadian Journal of Forest Research 31: 1940–1946.

12. Owensby, C. E., K. R. Blan, B. J. Eaton, and O. G. Russ. 1973. "Evaluation of Eastern Redcedar Infestations in the Northern Kansas Flint Hills." *Journal of Range Management* 26 (4): 256–260. URL: http://www.jstor.org/stable/3896570.

13. Slusher, J.P. (1995). "Wood Fuel for Heating." In University of Missouri Extension. URL: http://Extension.Missouri.Edu/Publications/Displaypub.Aspx?P=G5450

14. Starks, P. J., B. C. Venuto, J. A. Eckroat, and T. Lucas. (2011). "Measuring Eastern Red Cedar Juniperus Virginiana L. Mass with the Use of Satellite Imagery." *Rangeland Ecology & Management* 64 (2):178–186.

15. Stipe, D. J., and T. B. Bragg. (1989). "Effect of Eastern Red Cedar on Seedling Establishment of Prairie Plants." *Proceedings of the Eleventh North American Prairie Conference. 101–102*

16. Wylie, B. K., D. J. Meyer, M. J. Choate, L. Vierling, P. K. Kozak, And R. O. Green. (2000). "Mapping Woody Vegetation and Eastern Red Cedar in The Nebraska Sand Hills Using AVIRIS." Paper Read at AVIRIS Airborne Geoscience Workshop. JPL Publication 00-18. Pasadena, CA Jet Propulsion Laboratory, California Institute of Technology

Chapter 2 - A Comparison of Methods for the Assessment of Redcedar (Juniperus virginiana L.) Canopy Height Using LiDAR

2.1 Introduction

For over 50 years, the invasion of woody plant species into rangelands throughout the tallgrass prairie and surrounding regions has been a concern to ranchers and conservationists (Owensby, *et al*., 1972). Among the most prominent of these species is *Juniperus virginiana* L.; often called eastern redcedar (Owensby, *et al*., 1973; Norris, et al., 2001) (Figure 2.1). Eastern redcedar has a large range encompassing most of the eastern United States. (Norris, *et al*., 2001) The species is fast-growing and birds can transport its seeds over many miles. (Briggs, *et al*., 2002) Historically, before the widespread suppression of fire in the area, periodic burning of the prairie prevented eastern redcedar overexpansion. (Briggs and Gibson, 1992; Briggs, *et al*., 2002) Anthropogenic fire suppression has now resulted in the drastic expansion of its range. Throughout much of the Great Plains redcedar expansion has resulted in major economic losses due to a reduction in rangeland available for cattle grazing. In addition to economic losses, environmental impacts include loss of plant and animal community diversity and changes in nutrient cycling. Closed-canopy redcedar forest also presents a wildfire danger in areas where invasion occurs near suburban areas.

Figure 2-1 Eastern redcedar encroaching in a pasture near Russell, KS.

A potential solution to the problem of already-invaded areas is to find a large-scale commercial use for its biomass. Since eastern redcedar is a plentiful species that is "out of place" (Blatchley, 1912) in the prairie ecosystem, there is interest in harvesting redcedar stands for a variety of uses. Traditionally, redcedar wood has been used in fence posts and furniture, and it is commonly processed into mulch for gardening use. The wood can also be chipped and burned in wood-burning stoves or boilers, and methods are being developed to convert redcedar material into liquid biofuel products (Hemmerly, 1970; Lam, 2012; Ramachandriya, *et al.*, 2013).

Before redcedar can be harvested as a bio-fuel, it must be determined if there are enough dense stands in an area to make the establishment of infrastructure cost-efficient. In order to be cost efficient, it is best that large numbers of trees be clustered tightly together within an economically sustainable distance of processing facilities. While estimates of the overall scope of redcedar invasion and general estimates of biomass exist, there is little information on the spatial distribution of redcedar biomass within Kansas.

2.1.1 Assessment of Forest Biomass Using LiDAR

Studies have shown that Light Detection and Ranging (LiDAR) is a powerful tool for assessing forest biomass due to its ability to generate multiple returns (height measurements) within a single pulse when that pulse penetrates gaps in tree canopy (Figure 2.2).

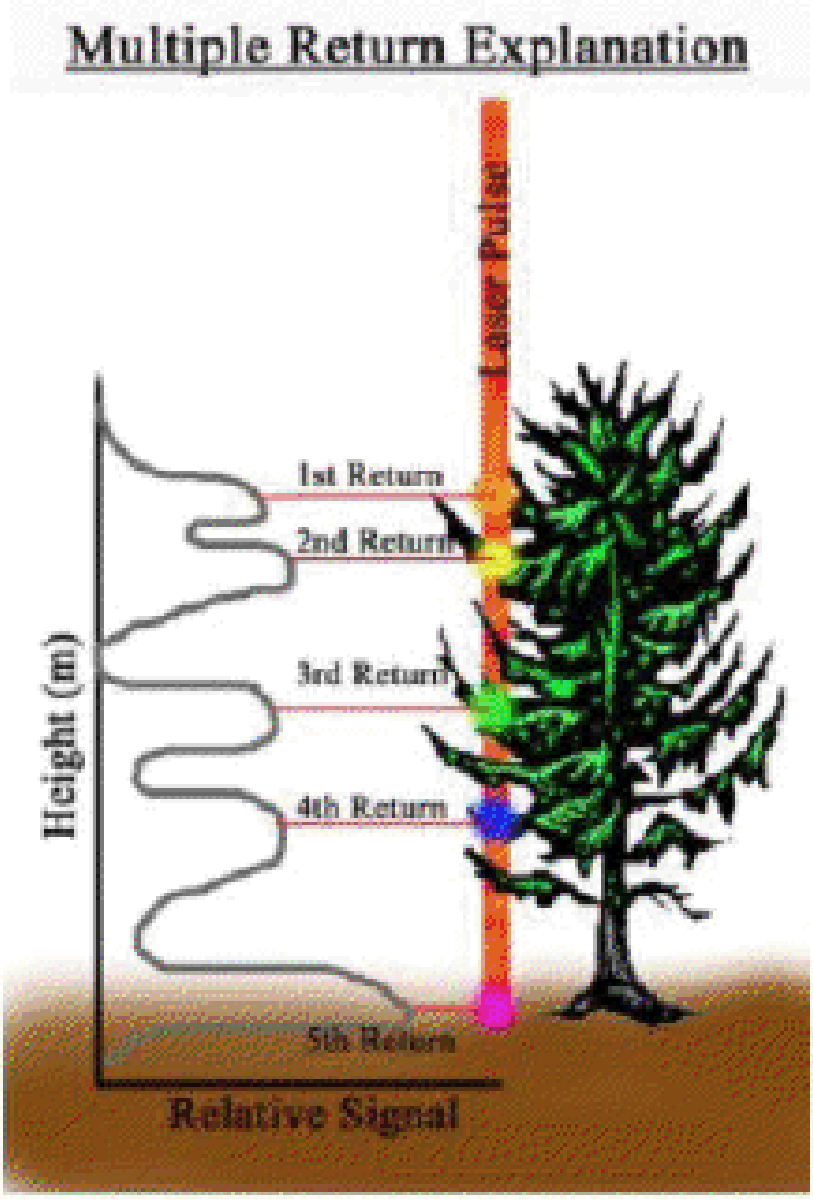

Figure 2-2 Illustration of multiple returns from a LiDAR pulse within a tree canopy. From Stoker (date unknown).

As a result, LiDAR data have been used extensively in surveys of native or highly managed forest stands. In 2003, Drake, *et al.* conducted a study where plot-level mean height of median energy derived from waveform LiDAR was combined with a linear regression technique to model aboveground biomass in neo-tropical forest. Popescu and Wynne (2004a) utilized a method of individual tree extraction based on a local maxima variable window approach. This method also utilized spectral data to differentiate between coniferous trees and deciduous trees when calculating window size based on a canopy-size-to-height ratio of the two tree types. In

2005, Bortolot and Wynne used an individual tree-based approach to estimate the biomass of a forest in Virginia. These studies all focused either on estimating biomass of single species in homogenous forest, or on estimating total aboveground biomass within a heterogeneous forest.

When an estimate of the biomass of a single tree species within a heterogeneous area is necessary, it is advantageous to combine LiDAR with multispectral imagery to differentiate biomass of different species. Recently, multiple attempts have been made to use LiDAR in conjunction with multispectral or hyperspectral imagery to map the biomass of invasive woody species in a mixed landscape. Swatantran, *et al.* (2011) found that incorporating hyperspectral classification improved their ability to predict biomass of a specific species when using waveform LiDAR in the Sierra Nevada. Another study utilized a data fusion of LiDAR and leaf-off ATLAS imagery to improve the performance of individual tree delineation and biomass estimation of deciduous and coniferous trees (Popescu & Wynne 2004b). These studies showed that the fusion of LiDAR and multispectral imagery can be beneficial for accurate biomass estimation of target species and tree types.

While a preponderance of the evidence points to a hybrid approach of using LiDAR and multispectral data to assess biomass of heterogeneous tree canopy, few studies have used this method on a large scale. Most studies have been on a stand level and not at larger county, region, or state levels. I found it beneficial, therefore, to conduct a preliminary investigation on which methods and approaches were most effective when mapping redcedar biomass at the county level. In order to determine the best method, it was initially decided to evaluate both a plot-level regression-based approach and an individual tree-based moving window approach. Along with the evaluation of these two approaches I endeavored to establish a methodology for integrating LiDAR data with multispectral data using available software and hardware resources.

A primary goal, therefore, was to compare the plot-level regression approach and the individual tree based approach to determine which method better predicted redcedar biomass using LiDAR. A secondary goal was to further confirm the efficacy of including multispectral imagery to better model the height of a target species (redcedar).

2.2 Methods

2.2.1 Study Area

Riley County, Kansas was selected as the study area for this project. The funding agency identified Riley County as a county of concern because of its high rate of redcedar encroachment. An unpublished study estimated a 23,000% increase of redcedar cover in Riley County between 1965 and 2005 (Grabow and Price, 2010).

Riley County lies within the Flint Hills ecoregion. Portions of the county are topographically rugged, with steep stream banks punctuating rocky upland areas. The native vegetation consists of tallgrass prairie species - primarily big bluestem (*Andropogon geradii*), Indiangrass (*Sorghastrum nutans*), and little bluestem (*Andropogon scoparius*) in the uplands - and trees—including hackberry (*Celtis occidentalis*), American elm (*Ulmus americana*), green ash (*Fraxinus pennsylvanica*), and black walnut (*Juglans nigra*) along the stream bottoms. The elevation ranges from 298 meters in the Kansas River Valley to 464 meters in the west-central portion of the county. Tuttle Creek Reservoir (along the Big Blue River) is a dominant feature in the county. Manhattan, the county seat and home of Kansas State University, is the largest city.

2.2.2 Collection of in-situ ground-reference data

Data collection, image classification, and canopy model assessment workflow is outlined in Figure 2.4. Seventeen ground-reference plots were selected throughout Riley County, Kansas across a redcedar cover and biomass gradient (Figure 2.3). Plots were approximately 15-meters by 15-meters for an approximate total area of 225 m^2 per plot. A GPS position was collected for the center of each plot and the four corners were measured out and situated at NE, NW, SE, and SW compass directions. The plots were digitized in ArcGIS® to facilitate extraction of percent cover metrics, derived from classification of multi-spectral imagery, and height metrics, derived from LiDAR, for each plot.

To characterize height, five trees were selected in each plot and height was calculated for each using a clinometer. The trees were selected using a modified point-center quarter method. In each plot, the tree closest to the center point and the trees closest to each of the four midpoints between the center and the four corners, were selected for height estimation and their locations within the plot were noted (Mitchell, 2010) (Figure 2.5). Tree age was also estimated for the selected trees by taking core samples using an increment borer. Densiometer measurements of

canopy density were taken in each of the four cardinal directions from each of the four midpoints. Densiometer measurements were averaged for each site. Biomass measurements were also collected for each site using diameter at breast height as a proxy. Site characteristics are summarized in Table 2.1.

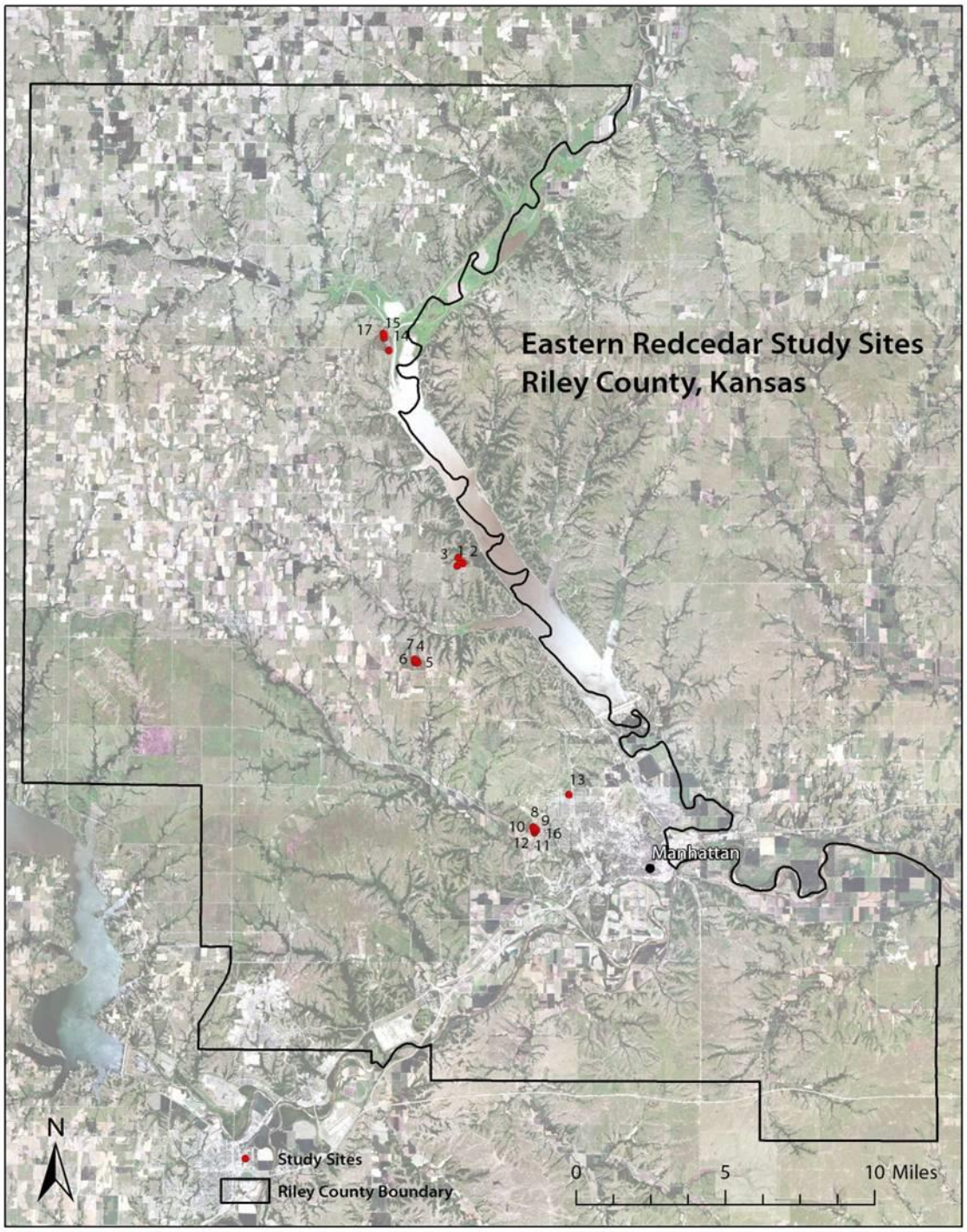

Figure 2-3 Map of Riley County, Kansas showing study plot locations in red.

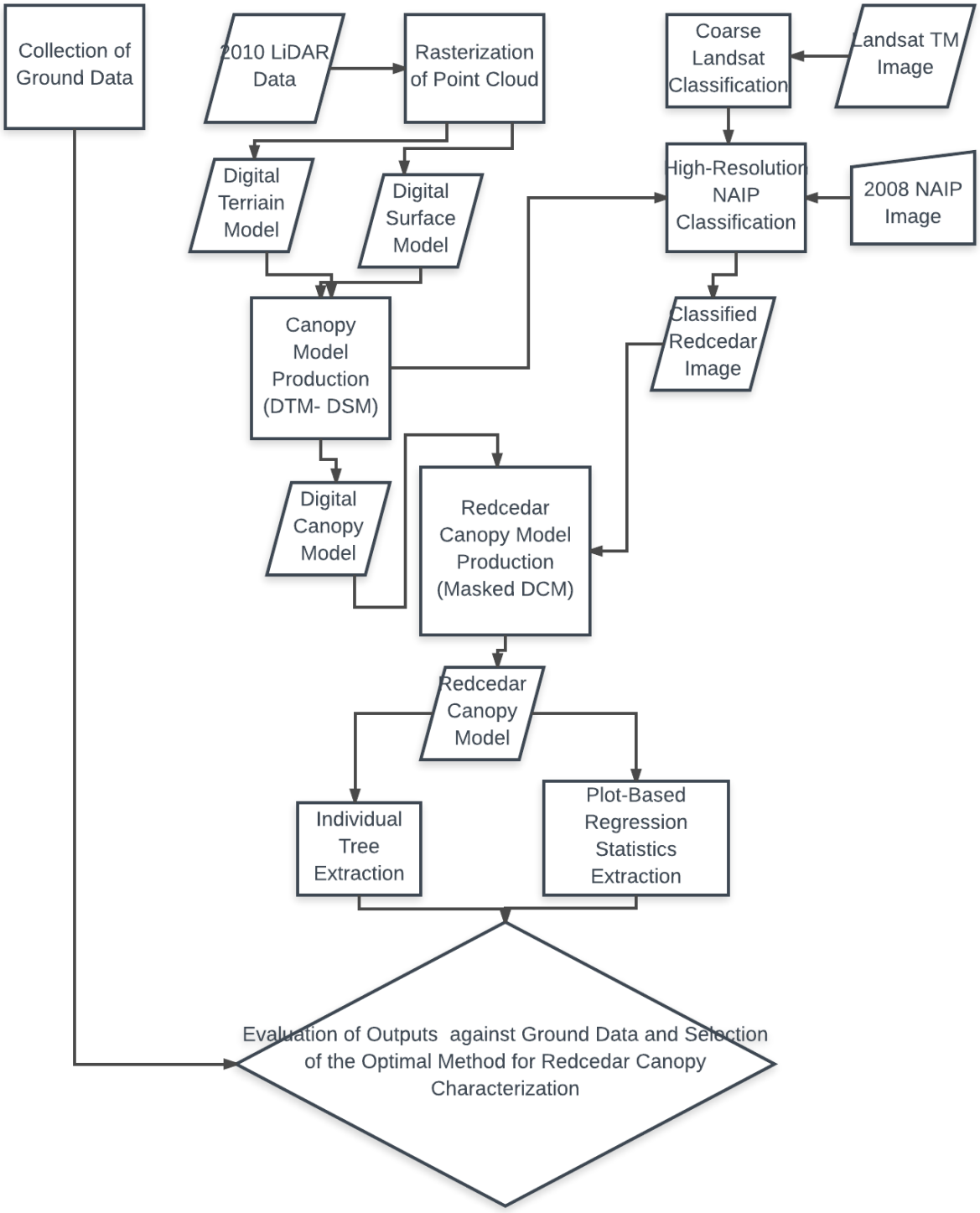

Figure 2-4 Redcedar Classification and Canopy Model Assessment Workflow.

Table 2-1 Summary of site measurements for each ground reference plot

Site	Average Age	Max Age	LiDAR Derived Canopy Height (m)	Ground Mean Tree Height (m)	Percent Cover Derived From Imagery	Densiometer Cover	Biomass (kg)
1	34.6	45	6.096	8.33	81.43%	92.24%	4992.73
2	30.25	40	2.902	7.70	46.94%	61.10%	2936.36
3	37	48	4.032	7.97	80.89%	81.44%	5288.64
4	29	43	2.76	7.91	50.00%	37.28%	3506.36
5	24	28	1.939	4.73	59.18%	42.22%	1595.00
6	N/A	N/A	4.335	8.42	79.59%	99.32%	3492.73
7	N/A	N/A	3.712	7.71	78.57%	86.84%	6008.64
8	N/A	N/A	4.112	7.45	53.57%	98.28%	5667.27
9	N/A	N/A	1.828	7.23	48.47%	61.20%	1955.91
10	N/A	N/A	0.911	4.61	16.84%	11.13%	686.82
11	N/A	N/A	0.919	4.05	17.86%	8.68%	410.45
12	N/A	N/A	2.063	6.24	47.96%	50.80%	2122.27
13	N/A	N/A	5.845	N/A	79.59%	89.39%	6467.73
14	N/A	N/A	2.669	5.60	54.08%	68.07%	2555.91
15	N/A	N/A	5.372	7.75	63.27%	75.30%	3670.00
16	N/A	N/A	1.1	4.42	11.73%	10.24%	395.91
17	N/A	N/A	1.699	4.76	22.45%	8.32%	859.09

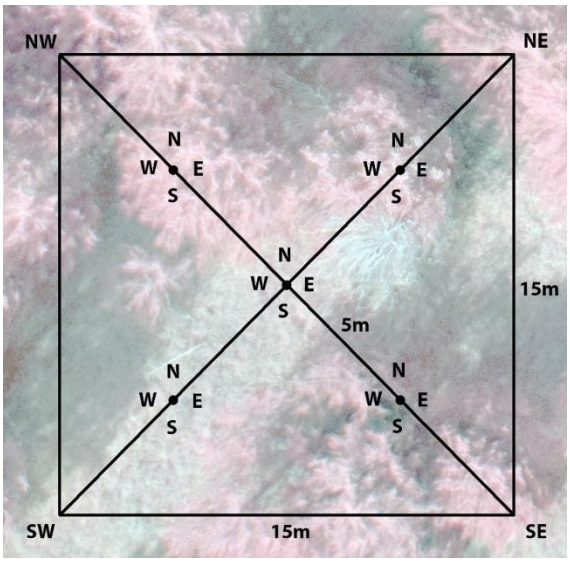

Figure 2-5 Aerial schematic of the modified point-center quarter sampling method at a study site.

2.2.3 LiDAR pre-processing

LiDAR data were obtained from the Kansas GIS Data Access Support Center (DASC) in .LAS format which contains the raw xyz coordinates of each point along with the return number. The dataset had been processed from its raw form which contains XYZ information along with sensor orientation, scan direction and range into LAS format projected in NAD 83 UTM Zone 15N by the vendor. Data were also classified into bare-earth returns versus all other returns by the distributer, however no further classification had been performed. Nominal point spacing was between 1.0 and 1.4 meters and vertical accuracy was approximately 18 centimeters. The LiDAR data were collected in spring of 2010.

LiDAR LAS files were processed using the Merrick® Advanced Remote Sensing software package (MARS®) provided to us for temporary use by Merrick Inc. The MARS® software has several different methods for raster interpolation from an LAS point cloud. (Merrick and Company, 2013) One method interpolates raster cell values from a triangulated representation of the point cloud generated as an intermediary. It was decided that this method was too computationally intensive and time consuming to be used. The other method uses a binning process to assign grid cell values from point values. When more than one value is

present the software allows the user to select whether to use a minimum, maximum, or average value. Gaps of less than 1-meter are then filled using a linear interpolation. Bare-earth and first-return rasters were created using this procedure, bare-earth returns were identified using the classification codes provided by the distributer, with the averaging option being selected for cells with multiple values. Both raster files were exported in the ESRI® grid format for import into ArcGIS®. Each was gridded at 1.0-meter per pixel resolution.

2.2.4 Classification of multispectral imagery

Two types of multispectral imagery were used to assess the range and density of redcedar for masking non-target species in the LiDAR derived canopy height model. Initially, a coarse (30-meter spatial resolution) Landsat classification was used to identify areas of redcedar cover. This classification ensured that areas of significant closed-canopy redcedar cover would be identified. It also provided a means of delineating the areas to be classified within the higher resolution data. The second round of multispectral classification involved the hybrid use of U.S. Department of Agriculture National Agricultural Imagery Program (NAIP) 4-band (NIR-R-G-B) data and LiDAR. Within areas already identified as containing redcedar based on the coarser Landsat classification, a second classification was derived from the higher resolution NAIP data. This allowed for a more accurate estimate of redcedar density. The resulting 1.0-meter spatial resolution classification of redcedar was subsequently used to identify the target species in a 1-meter LiDAR-derived canopy height model (Figure 2.6).

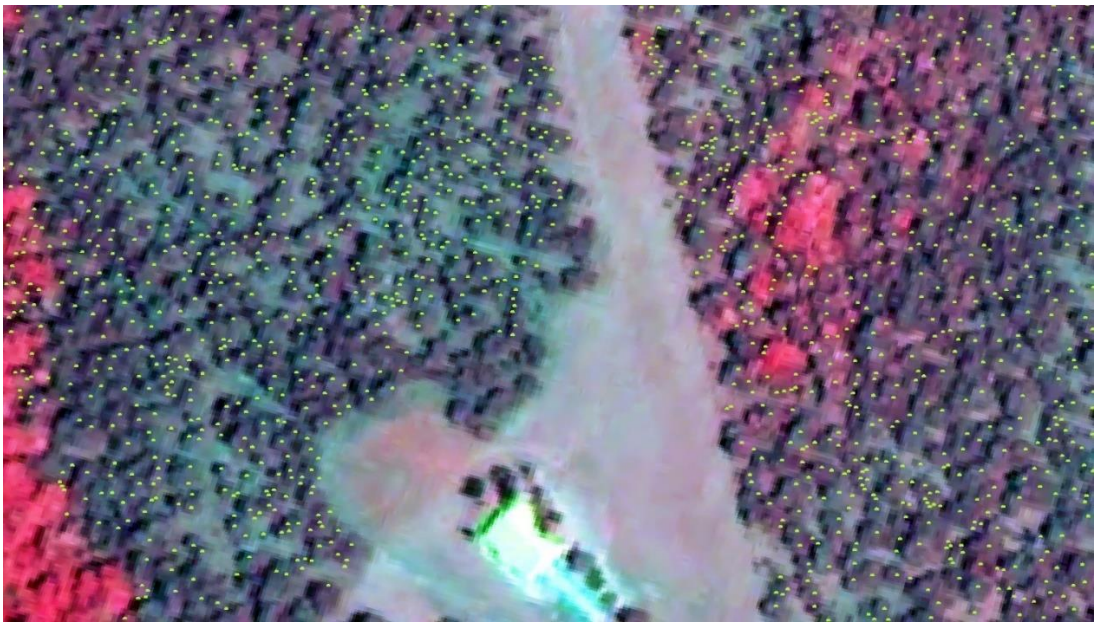

Figure 2-6 1.0 Meter NAIP color-infrared orthoimagery showing spectral distinction between decidious and redcedar tree canopy.

2.2.4.1 Unsupervised classification of Landsat Imagery

A multi-temporal classification technique was performed using cloud-free Landsat TM images from January 5, 2011 and August 1, 2011, representing winter and summer dates, respectively. Six bands from each image (omitting the thermal band) were stacked using ERDAS Imagine© software. The resulting 12-band image (see Figure 2.7) was used as the input in the ISODATA unsupervised classifier tool in ERDAS Imagine. An Output settings were set to 50 clusters with a confidence interval of 0.95. The resulting 50 spectral clusters were manually interpreted by comparing them with ground truth data and high-resolution NAIP imagery. A modified Anderson Level I classification scheme (Anderson, 1976) was to classify each cluster. The Level I "forest land" class was split into "deciduous forest land" and "evergreen forest land" as indicated in level 2 of the Anderson scheme. This separation was preferred since evergreen forest in the study area is almost exclusively comprised of eastern redcedar, the target land cover type.

The clusters that were interpreted to include redcedar cover were identified and extracted using ISODATA. An iterative process known as "cluster busting" was used to further refine the redcedar classification (Jensen, 2005). During cluster busting, the analyst identifies the clusters that include or that are most spectrally similar to the target land cover type. All other clusters are

masked out, and ISODATA is performed a second time. This application of this process often reveals "hidden" spectral information that can reveal other land cover types in the image that were not evident in the initial ISODATA classification. Multiple iterations of cluster busting are sometimes necessary to accurately extract a particular land cover type, as was the case in extracting redcedar cover. For this study, two iterations were necessary to separate redcedar from other cover types. After redcedar was accurately classified, the classification accuracy was assessed using a simple random sampling scheme to visually compare the classified Landsat pixels with high resolution NAIP imagery in which redcedar cover was more obvious.

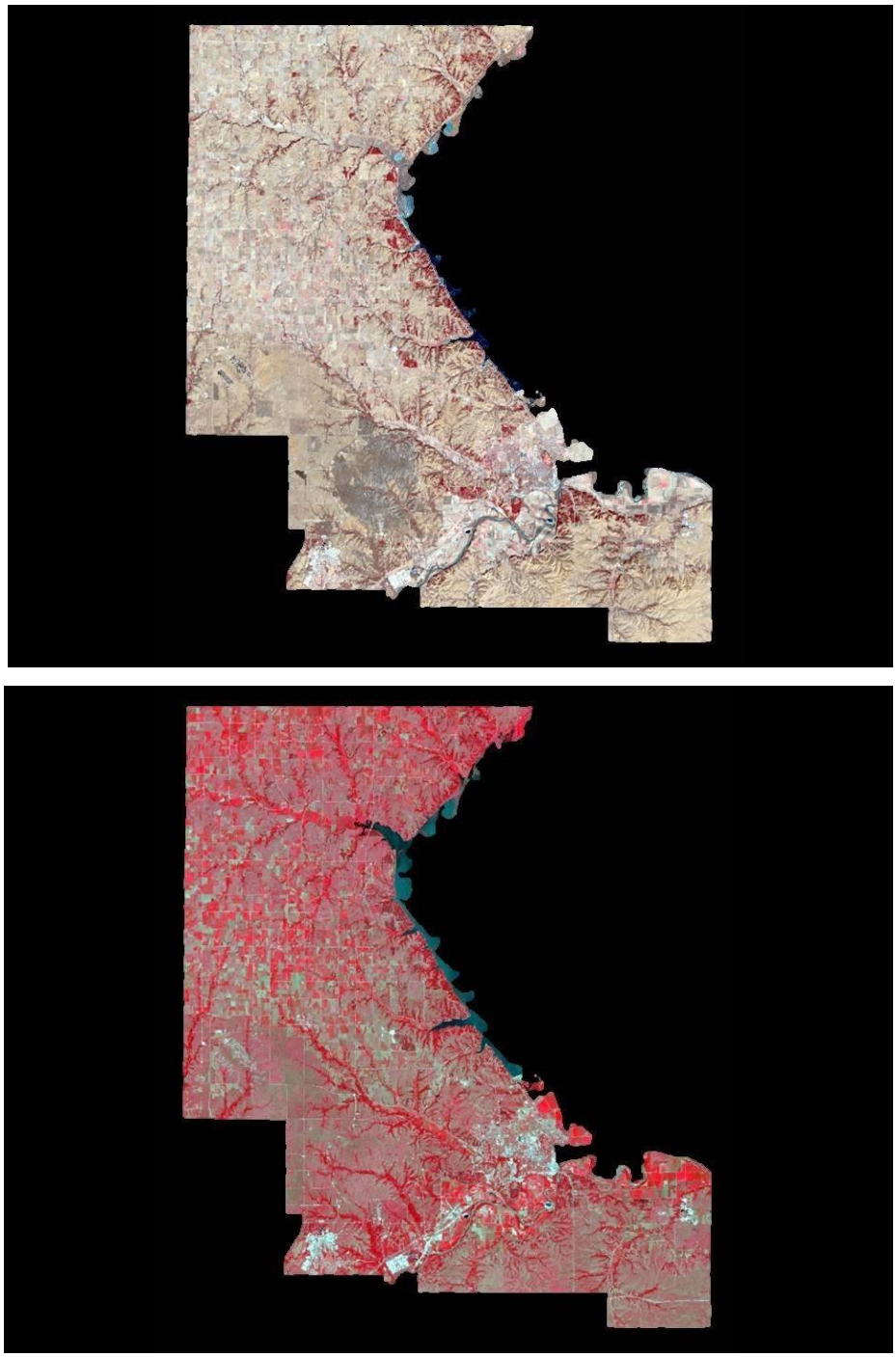

Figure 2-7 False-color composite (4-3-2) Landsat TM images of Riley County, Kansas from January 5, 2011 (top) and August 1, 2011 (bottom).

2.2.4.2 Classification of higher spatial resolution NAIP Imagery

USDA NAIP 4-band data from 2008 were obtained from the Kansas Data Access Support Center (DASC). NAIP data were not available with a near-infrared band in the raw format for the same period as the LiDAR collection and therefore, a decision was made to use the closest possible collection. The spatial resolution of the data was 1.0-meter and the data had been orthorectified Multispectral data were co-registered to the LiDAR canopy models to ensure proper alignment (RMS error less than one pixel). Prior to classification of NAIP data, all areas within the imagery corresponding with areas in the canopy height model below 0.5 meters were masked out. This removed any remaining water pixels and shadow on the ground, both of which were easily confused with dark shadowed redcedar spectral values in the data. An unsupervised classification was then conducted for all areas classified as redcedar in the initial Landsat classification.

Once again, the ISODATA classification algorithm was used to produce 50 clusters. Clusters were visually interpreted and assigned to redcedar and non-redcedar classes. User's accuracy was calculated using 100 randomly selected validation samples that were evaluated using a combination of site survey and imagery interpretation. Percent cover by redcedar was calculated from the classified NAIP data for each of the 17 study sites using the ArcGIS® zonal statistics tool.

2.2.5 Redcedar canopy model development

Development of a canopy model representative of redcedar only necessitated the removal of other aboveground structures and tree species from the canopy height raster. This was accomplished using a 1.0-meter resolution redcedar binary mask created from the classified high-resolution image data. The application of this mask resulted in a canopy height model representative of only redcedar canopy height.

2.2.6 Comparison of Individual Tree Based Approach versus Plot-Level Regression for Assessment of Redcedar Biomass

The two LiDAR-based methods of assessing redcedar biomass were compared to ground reference data to determine which produced a better predictive model.

To test the plot-level regression approach, the ArcGIS® zonal statistics tool was used to calculate the summary statistics of the canopy height model for each of the 17 study sites: sum of canopy height, mean canopy height, median canopy height, maximum canopy height, minimum canopy height, and standard deviation of canopy height. Zeros were not included in the calculation of zonal statistics pertaining to the canopy height model. The exclusion of zeros allowed for the calculation of a more accurate measure of mean canopy height.

Testing the individual tree-based approach proved more challenging. This method involves passing a moving window through the derived canopy height model to identify individual trees (Popescu and Wynne, 2004a). A circular window with a variable radius is used to identify local maxima which are identified as tree tops. The corresponding local minima are identified as the base height. The window size is calculated using an equation based on the relationship between tree height and canopy width. The allometric equation, developed using data collected at the study sites, is illustrated in Figure 2.8. To test this method, the moving window algorithm was evaluated using a subset of the 17 study plots. It was decided to use a subset because of the computational intensity of the process and the need to determine if the method yielded accurate tree level statistics before testing it on a larger area. This was accomplished using the Canopy Maxima algorithm implemented in the Fusion software provided by the US forest service. This algorithm is like that reported in Popescu and Wynn (2004b).

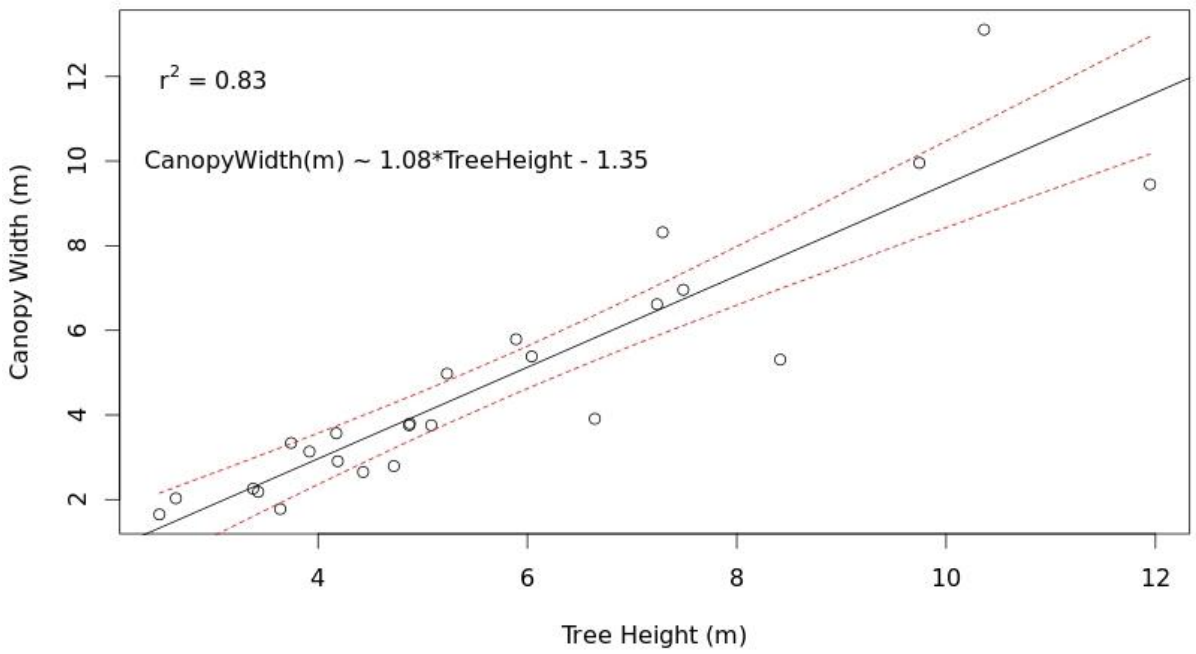

Figure 2-8 Allometric equation, developed from field data collected at our study sites, relating redcedar canopy width to tree height. This equation was used as an input for the local-maxima based individual tree filter.

2.3 Results

2.3.1 Plot-Level Regression Model

The relationship between the plot-level mean height of the redcedar canopy height model based on LiDAR data and the mean tree height of selected trees in ground reference plots can be seen in the graph in Figure 2.9. The model is precise ($r^2 = 0.77$, $p \leq 0.05$) however there is considerable bias y-intercept > 4 meters. The Root Mean Squared Error of the model was calculated to be 0.74 meters. While a bias is present and some error exists the precision of this relationship suggests that LiDAR be used to model redcedar canopy height if the bias is considered.

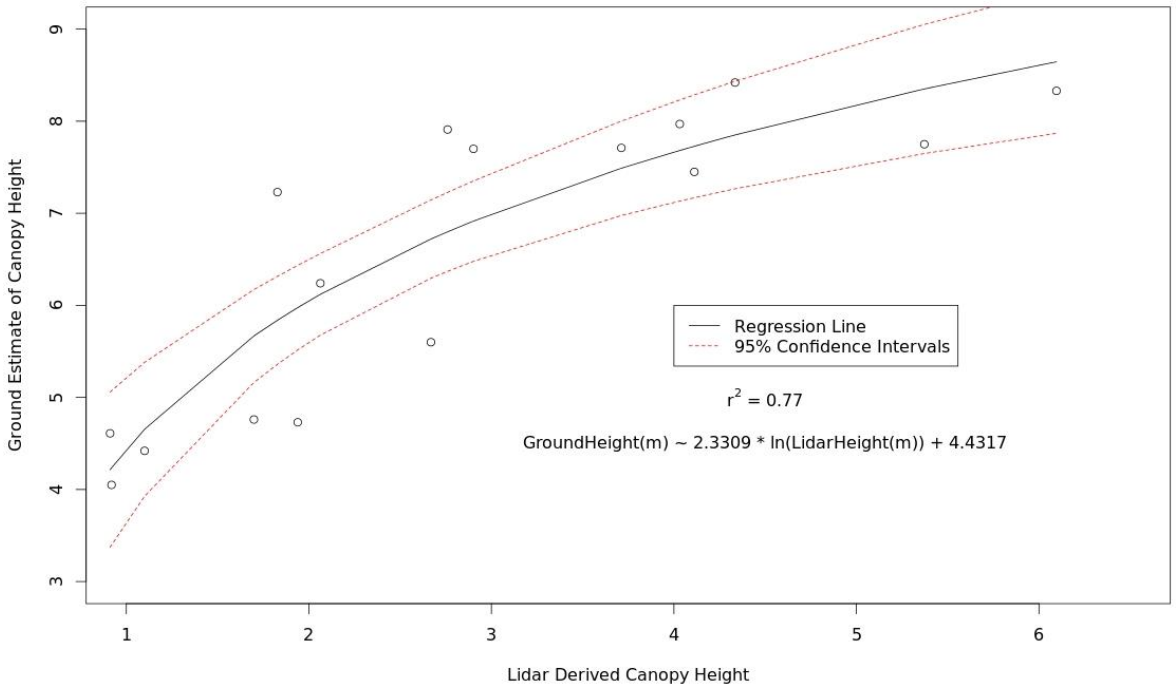

Figure 2-9 Redcedar canopy height model (LiDAR) vs. mean redcedar height in ground reference plots.

2.3.2 Individual Tree Based Model

As indicated in Figure 2.10 the moving window individual tree-based method produced mixed results in identifying single trees. In circumstances where the trees were physically separated from surrounding trees the model identified tree tops with a reasonable degree of accuracy. When the canopies of multiple trees coalesced, however, the tree tops were not reliably identified, resulting in an overall under-representation of the number of trees.

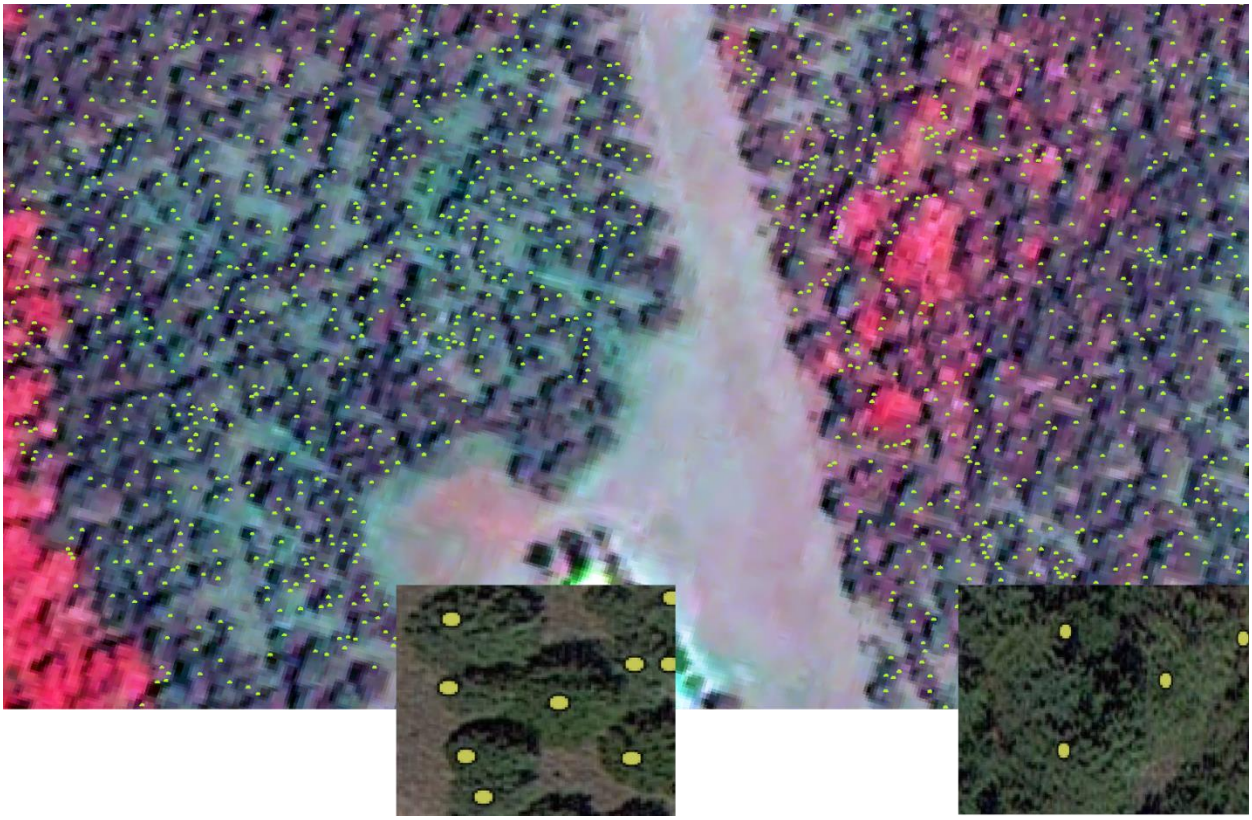

Figure 2-10 Results of individual tree identification model, the points represent individual tree tops identified by the model. Points are superimposed over CIR NAIP imagery used in classification. Subsets show model results with somewhat separated trees vs. coalescent canopy.

2.4 Discussion and Conclusions

2.4.1 Optimal Method for Assessment of Redcedar Biomass and Canopy Characteristics

The results presented in this chapter indicate that a plot-level regression approach is favorable for accessing redcedar biomass and canopy characteristics. This is mostly due to the computational intensity of an individual tree-based approach and the inability of such an approach to properly characterize the canopy characteristics of redcedar. The computational intensity of the individual tree-based approach alone prevents it from being practical for county or region-wide assessment.

2.4.2 Sources of Error and Potential for Improved Models

2.4.2.1 Error in the Individual Tree Based Model

One potential source of error is the point spacing of the LiDAR as well as the complexities of redcedar canopy structure. Coalescent redcedar canopy and a wide variety of canopy geometries across redcedar specimens may have played a role. As the technology improves, however, tighter point spacing will become feasible at lower costs. Tighter point LiDAR spacing could allow for better characterization of crown shape, thereby allowing the re-evaluation of individual tree-based approaches for certain applications. Another potential source of error are the incongruences between collection time of field data and of remotely sensed data. Factors such as growth of the trees between data collection or removal of trees could have contributed to error.

Future work includes expanding the study to other areas prone to redcedar encroachment, improving model accuracy by simultaneous collection of ground reference and remotely sensed data, and exploring other LiDAR-based forest inventory techniques, such as individual tree extraction.

2.4.2.2 Error in the Plot-Based Regression Model

The bias in this relationship could be related to the inherit accuracy of the LiDAR data which has a vertical RMSE of +/- 0.18 meters combined with the three year gap between LiDAR and ground/multispectral data acquisition. Sense the plot-based regression approach summarizes the height of all grid cells within a plot given a single number it is possible that there will always be some bias sense lower level canopy returns will reduce the height estimate. A more robust model might incorporate the variability of the canopy height model within the plot.

Although there is some error in the plot-based regression approach when it comes to height estimation the accuracy of the final biomass model, discussed in depth in chapter 3, was in line with previous studies using LiDAR to model tree biomass (Drake *et al.*, 2003). Having a root-mean squared error of approximately 35 megagrams (metric tons) per hectare, the model results support the use of a plot-level regression-based approach for accessing redcedar biomass and canopy characteristics.

References

1. Anderson, J. R., E. E. Hardy, J. T. Roach, and R. E. Witmer. 1976. *A Land Use and Land Cover Classification System for Use with Remote Sensor Data*. Washington, D.C.: United States Government Printing Office.

2. Briggs, J. M., and D.J. Gibson. 1992. "Effect of Burning on Tree Spatial Patterns in a Tallgrass Prairie Landscape." *Bulletin of the Torrey Botanical Club* 119: 300–307.

3. Briggs, J. M., G. A. Hoch, and L. C. Johnson. 2002. "Assessing the Rate, Mechanisms, and Consequences of the Conversion of Tallgrass Prairie to Juniperus Virginiana Forest." *Ecosystems*. 5 (6): 578–586.

4. Briggs, J. M., A. K. Knapp, and B. L. Brock. 2002. "Expansion of Woody Plants in Tallgrass Prairie: A Fifteen-Year Study of Fire and Fire-Grazing Interactions." *American Midland Naturalist* 147 (2): 287–294.
URL: http://www.jstor.org/stable/3083203.

5. Bortolot, Z. J., and R. H. Wynne. 2005. "Estimating Forest Biomass Using Small Footprint LiDAR Data: an Individual Tree-Based Approach That Incorporates Training Data." *ISPRS Journal of Photogrammetry and Remote Sensing* 59 (6): 342–360.

6. Coppedge, B. R., D. M. Engle, R. E. Masters, and M. S. Gregory. (2001). "Avian Response to Landscape Change in Fragmented Southern Great Plains Grasslands." *Ecological Applications* 11 (1): 47–59.

7. Chapman, R. N., D. M. Engle, R. E. Masters, and D. M. Leslie Jr. (2004) "Tree Invasion Constrains the Influence of Herbaceous Structure in Grassland Bird Habitats." *Ecoscience* 11 (1): 56–63.

8. Drake, J. B., R. G. Knox, R. O. Dubayah, D. B. Clark, R. Condit, J. B. Blair, And M. Hofton. (2003). "Above-Ground Biomass Estimation in Closed Canopy Neotropical Forests Using Lidar Remote Sensing: Factors Affecting the Generality of Relationships." *Global Ecology and Biogeography* 12 (2): 147–159.

9. Harwin, Steve, and Arko Lucieer. "Assessing the accuracy of georeferenced point clouds produced via multi-view stereopsis from unmanned aerial vehicle (UAV) imagery." Remote Sensing 4, no. 6 (2012): 1573-1599.

10. Horncastle, V. J., E. C. Hellgren, P. M. Mayer, A. C. Ganguli, D. M. Engle, And D. M. Leslie Jr. (2005) "Implications of Invasion by Juniperus Virginiana on Small Mammals in The Southern Great Plains." *Journal of Mammalogy* 86 (6): 1144–1155.

11. Jensen, J. R. 2005. *Introductory Digital Image Processing: A Remote Sensing Perspective*. Upper Saddle River: Pearson Prentice Hall.

12. Lucas, R. M., N. Cronin, A. Lee, M. Moghaddam, C. Witte, and P. Tickle. (2006). "Empirical Relationships between AIRSAR Backscatter and Lidar-Derived Forest Biomass, Queensland, Australia." *Remote Sensing of Environment* 100 (3):407–425.

13. Norris, M., J. Blair, L. Johnson, and R. Mckane. (2001). "Assessing Changes in Biomass, Productivity, and C and N Stores Following Juniperus Virginiana Forest Expansion into Tallgrass Prairie" Canadian Journal of Forest Research 31: 1940–1946.

14. Owensby, C. E., K. R. Blan, B. J. Eaton, and O. G. Russ. 1973. "Evaluation of Eastern Redcedar Infestations in the Northern Kansas Flint Hills." *Journal of Range Management* 26 (4): 256–260. URL: http://www.jstor.org/stable/3896570.

15. Popescu, S. C., and R. Wynne. (2004a). "Seeing the Trees in The Forest: Using Lidar and Multispectral Data Fusion with Local Filtering and Variable Window Size for Estimating Tree Height." *Photogrammetric Engineering and Remote Sensing* 70 (5):589-604.

16. Popescu, S. C., R. H. Wynne, and J. A. Scrivani. (2004b). "Fusion of Small-Footprint Lidar and Multispectral Data to Estimate Plot-Level Volume and Biomass in Deciduous and Pine Forests in Virginia, USA." *Forest Science* 50 (4): 551–565.

17. Slusher, J.P. (1995). "Wood Fuel for Heating." In University of Missouri Extension. URL: http://Extension.Missouri.Edu/Publications/Displaypub.Aspx?P=G5450

18. Starks, P. J., B. C. Venuto, J. A. Eckroat, and T. Lucas. (2011). "Measuring Eastern Red Cedar Juniperus Virginiana L. Mass with the Use of Satellite Imagery." *Rangeland Ecology & Management* 64 (2):178–186.

19. Stipe, D. J., and T. B. Bragg. (1989). "Effect of Eastern Red Cedar on Seedling Establishment of Prairie Plants." *Proceedings of the Eleventh North American Prairie Conference. 101–102*

20. Swatantran, A., R. Dubayah, D. Roberts, M. Hofton, and J. B. Blair. (2011). "Mapping Biomass and Stress in The Sierra Nevada Using Lidar and Hyperspectral Data Fusion." *Remote Sensing of Environment* 115 (11): 2917–2930.

21. Triggs, Bill, Philip F. McLauchlan, Richard I. Hartley, and Andrew W. Fitzgibbon. "Bundle adjustment—a modern synthesis." In *Vision algorithms: theory and practice*, pp. 298-372. Springer Berlin Heidelberg, 1999.

22. Wylie, B. K., D. J. Meyer, M. J. Choate, L. Vierling, P. K. Kozak, And R. O. Green. (2000). “Mapping Woody Vegetation and Eastern Red Cedar in The Nebraska Sand Hills Using AVIRIS.” Paper Read at AVIRIS Airborne Geoscience Workshop. JPL Publication 00-18. Pasadena, CA Jet Propulsion Laboratory, California Institute of Technology

Chapter 3 - Assessment of Eastern Redcedar (*Juniperus virginiana*) Biomass Using LiDAR and Multispectral Imagery[2]

3.1 Introduction

For over 50 years, the invasion of woody plant species into rangelands throughout the tallgrass prairie ecoregion has been a serious concern to ranchers and conservationists (Owensby, *et al.*, 1973). Among the most prominent of these species is *Juniperus virginiana* L., often called eastern redcedar (Owensby, *et al.*, 1973; Norris, *et al.*, 2001) (Figure 3.1). Eastern redcedar has a large range encompassing most of the eastern United States. (Norris, *et al.*, 2001) The species is fast-growing, and birds can transport its seeds over many miles (Briggs, *et al.*, 2002). Historically, prior to the widespread suppression of natural prairie fires in the region, periodic burning of the prairie prevented eastern redcedar overexpansion (Briggs and Gibson, 1992; Briggs, *et al.*, 2002). Anthropogenic fire suppression has now resulted in the drastic expansion of its range (Strine, 2004; Owensby, *et al.*, 1973). In much of the Great Plains, this expansion has become an economic threat to the cattle ranching industry due to the loss of rangeland available for cattle grazing (Schmidt, 2002). Along with economic impacts caused by redcedar expansion, there are also environmental impacts, including losses in plant and animal community diversity (Chapman, 2004; Horncastle, 2005; Briggs, *et al.*, 2002). Closed-canopy redcedar forests also present a wildfire danger where redcedar expansion occurs near urban areas (Ward, 2013).

A potential solution to the problem of redcedar invasion is to find a large-scale commercial use for redcedar biomass. Since eastern redcedar is a plentiful species that is "out of place" (Blatchley, 1912) in the prairie ecosystem, there has been interest in harvesting redcedar stands for a variety of uses. Traditionally, redcedar wood has been used in fence posts and furniture, and it is commonly turned into mulch for gardening use. The wood can also be chipped and burned in wood-burning stoves or boilers, and methods are being developed to convert redcedar material into liquid biofuel products (Hemmerly, 1970; Lam, 2012; Ramachandriya, *et al.*, 2013). Redcedar oil has also been utilized in the essential oil industry and reportedly has

[2] Chapter Co-Authored with and Reprinted with Permission from David Burchfield

antibacterial and anti-cancer properties (Gawde, *et al.*, 2009; CAFNRnews, 2008; Semen & Hiziroglu, 2005).

Figure 3-1 Eastern redcedar in Riley County, Kansas.

Before redcedar can be harvested for use as a biofuel or other product, it must be determined if there is enough redcedar biomass in an area to allow a harvesting industry to be economically viable in that area, especially considering the costs of transporting the trees from harvest locations to a refinery. For harvesting to be cost-effective, it is best that large numbers of trees be clustered tightly together within an economically sustainable distance of processing facilities. While estimates of the overall scope of redcedar invasion and general estimates of biomass exist (Grabow and Price, 2010; Moser, *et al.*, 2008), there is little information on the spatial distribution of redcedar biomass within Kansas. Currently available redcedar biomass information, collected using a random ground sampling technique (Bechtold & Patterson, 2005), has been shown in many cases to be inaccurate at a county level.

Considering eastern redcedar's detrimental environmental and economic impacts, as well as its potential commercial benefits, two major objectives were identified for this project. The primary objective was to establish an allometric equation using various plant metrics (diameter at breast height and tree height) to predict redcedar biomass at the individual tree and study plot ($225m^2$) levels. The secondary objective was to use LiDAR imagery, along with multispectral image data, to classify redcedar stands and estimate redcedar biomass across a large area (*e.g.* county).

3.1.1 Use of LiDAR and multispectral imagery in forest inventories

While there are general volumetric and areal estimations of redcedar invasion, there is little information on the exact spatial extent and density of biomass. To determine the cost-benefit of redcedar harvest, there must be accurate estimates of standing biomass within areas under consideration for harvest operations. Multispectral imagery has been used in the past to assess redcedar extent and biomass. Wylie *et al.* (2000) used Airborne Visible/Infrared Imaging Spectrometer (AVIRIS) data to map eastern redcedar in the Nebraska sand hills. Starks, *et al.* (2011) found a strong correlation between derived metrics from high-resolution satellite imagery (0.42 m/pixel) and aboveground redcedar biomass.

In addition, studies have shown that Light Detection and Ranging (LiDAR) is a powerful tool for assessing forest biomass due to its ability to generate multiple returns (height measurements) within a single pulse when that pulse penetrates gaps in tree canopy (Figure 3.2). Thus, LiDAR data have been used extensively in surveys of native or highly managed forest stands. In 2003, Drake, *et al.* conducted a study where plot-level mean height of median energy derived from waveform LiDAR was combined with a linear regression technique to model aboveground biomass in neo-tropical forest. Popescu and Wynne (2004a) utilized a method of individual tree extraction based on a local maxima variable window approach. This method also utilized spectral data to differentiate between coniferous trees and deciduous trees when calculating window size based on a canopy-size-to-height ratio of the two tree types. In 2005, Bortolot and Wynne used an individual tree-based approach to estimate the biomass of a forest in Virginia. These studies all focused on either estimating biomass of single species in homogenous forest, or estimation of total aboveground biomass within a heterogeneous forest. When an estimate of the biomass of a single tree species within a heterogeneous area is necessary, it

becomes advantageous to combine LiDAR with multispectral imagery to differentiate biomass of different species. Recently, multiple attempts have been made to use LiDAR in conjunction with multispectral or hyperspectral imagery to map the biomass of invasive woody species in a mixed landscape. Swatantran, *et al.* (2011) found that incorporating hyperspectral classification improved their ability to predict biomass of a specific species when using waveform LiDAR in the Sierra Nevada. Another study utilized a data fusion of LiDAR and leaf-off ATLAS imagery to improve the performance of individual tree delineation and biomass estimation of deciduous and coniferous trees (Popescu & Wynne 2004b). These studies showed that the fusion of LiDAR and multispectral imagery can be beneficial for accurate biomass estimation of target species and tree types.

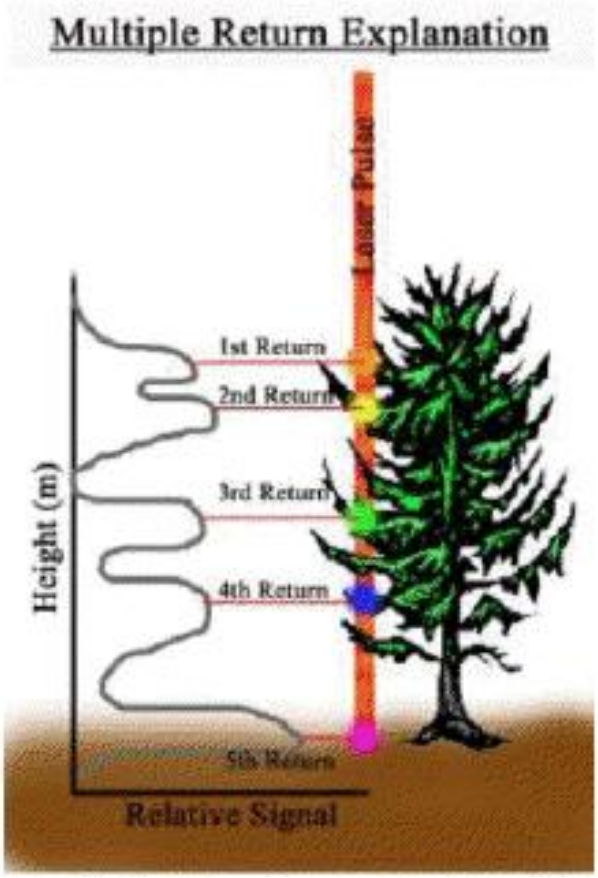

Figure 3-2 Illustration of multiple returns from a LiDAR pulse within a tree canopy. From Stoker (date unknown).

For this project, a plot-based regression technique utilizing LiDAR-derived canopy height, together with a classification derived from multispectral data, was chosen rather than an

individual tree-based approach. The reasons for this hybrid methodology include the relatively sparse point spacing of the available LiDAR data (1.4 meters) and the variable nature of redcedar tree crown shape. Window size calculations necessary for individual tree extraction require knowledge of crown structure and differ by tree species. Redcedar trees can show a wide variety of crown structures (*e.g.* ranging from conic or columnar), making individual tree extraction problematic when attempted over large areas.

3.2 Methods

3.2.1 Study Area

The project study area, Riley County, Kansas, was identified by the Kansas Forest Service as a county of concern due to its high rate of redcedar encroachment. An unpublished study estimated a 23,000% increase of redcedar cover in Riley County between 1965 and 2005 (Grabow & Price, 2010). Riley County lies within the Flint Hills ecoregion. Portions of the county are topographically rugged, with steep stream banks punctuating rocky upland areas. The native vegetation consists of tallgrass prairie species—primarily big bluestem (*Andropogon gerardii*), indiangrass (*Sorghastrum nutans*), and little bluestem (*Andropogon scoparius*)—in the uplands. Trees, including hackberry (*Celtis occidentalis*), American elm (*Ulmus americana*), green ash (*Fraxinus pennsylvanica*), and black walnut (*Juglans nigra*) are found along the stream bottoms (Owensby, 2014). The elevation ranges from 298 meters in the Kansas River Valley to 464 meters in the west-central portion of the county. Tuttle Creek Reservoir (along the Big Blue River) is a dominant feature in the county. Manhattan, the county seat and home of Kansas State University, is the largest city. The total area of the county is 1611 km^2 (U.S. Census Bureau, 2013), most which is utilized for cattle grazing and crop production. The climate in Riley County is classified as humid continental (Köppen *Dfa*) (Peel, *et al.*, 2007).

3.2.2 Collection of in situ ground reference data

Data collection, image classification, and biomass assessment workflow is outlined in Figure 3.3. *In situ* data from 17 ground reference plots was collected throughout Riley County, Kansas across a redcedar cover and biomass gradient (Figure 3.5). Plots were approximately 15 by 15 meters for an approximate total area of 225 m^2 per plot. A GPS position was collected for the center of each plot and the four corners were measured out and situated at NE, NW, SE, and

SW compass directions. The plots were digitized in ArcGIS® to facilitate extraction of percent cover metrics (derived from classification of multispectral imagery) and height metrics derived from LiDAR for each plot.

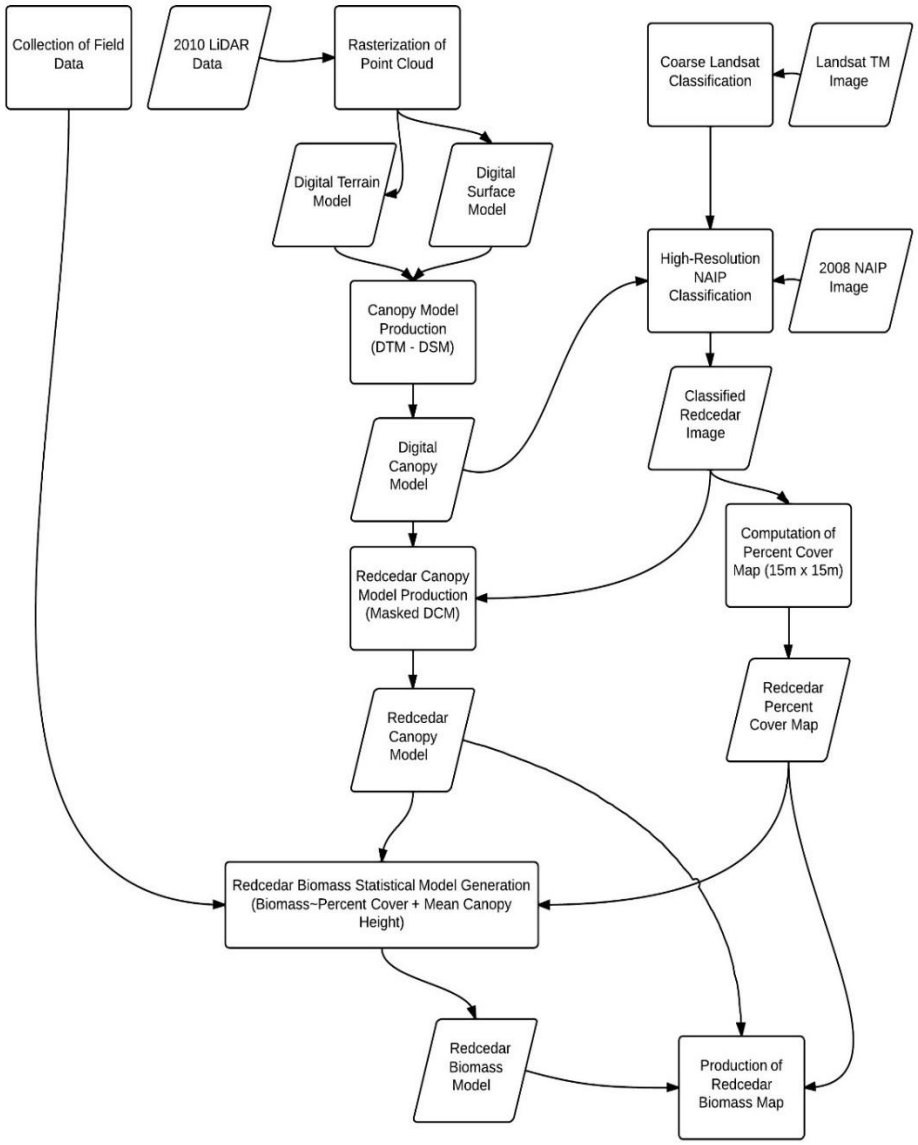

Figure 3-3 Redcedar classification and biomass mapping workflow.

Biomass was estimated for each tree within the plot using diameter at breast height (DBH) as an input into an allometric equation based on our own data and data collected by the

students of the Kansas State University Natural Resources and Environmental Sciences capstone course (Strauss *et al.*, 2011). DBH has been found to be a reliable predictor of individual tree total aboveground biomass when it is not possible to weigh each tree, as illustrated in Figure 3.4. A similar equation was used by Norris, *et al*. (2001) to estimate redcedar biomass. Total biomass estimates for each plot were calculated by summing the estimated biomass of every tree with a DBH of greater than two inches. The two-inch threshold was chosen because trees with DBH smaller than two inches were considered to have negligible biomass from a harvest standpoint and were also considered too small to be easily detectable in the aerial image data used in this project (1.0-meter spatial resolution). Age and height estimates of five trees in each plot were also collected to further characterize the sites and for validation of remotely sensed height models. These trees were selected using a modified point-center quarter method. In each plot, the tree closest to the center point and the trees closest to each of the four midpoints between the center and the four corners were selected for height and tree age estimation and their locations within the plot were noted (Mitchell, 2010) (Figure 3.6). Height was calculated using a clinometer, and tree age was estimated for some sites by taking core samples using an increment borer. (It was quickly realized that tree age would not improve biomass prediction, so average ages were not calculated for all sites.) Canopy density was measured using a densiometer facing each of the four cardinal directions from each of the four midpoints. Densiometer measurements were averaged for each site and used to help validate remotely sensed percent cover estimates. Site characteristics are summarized in Table 3.1.

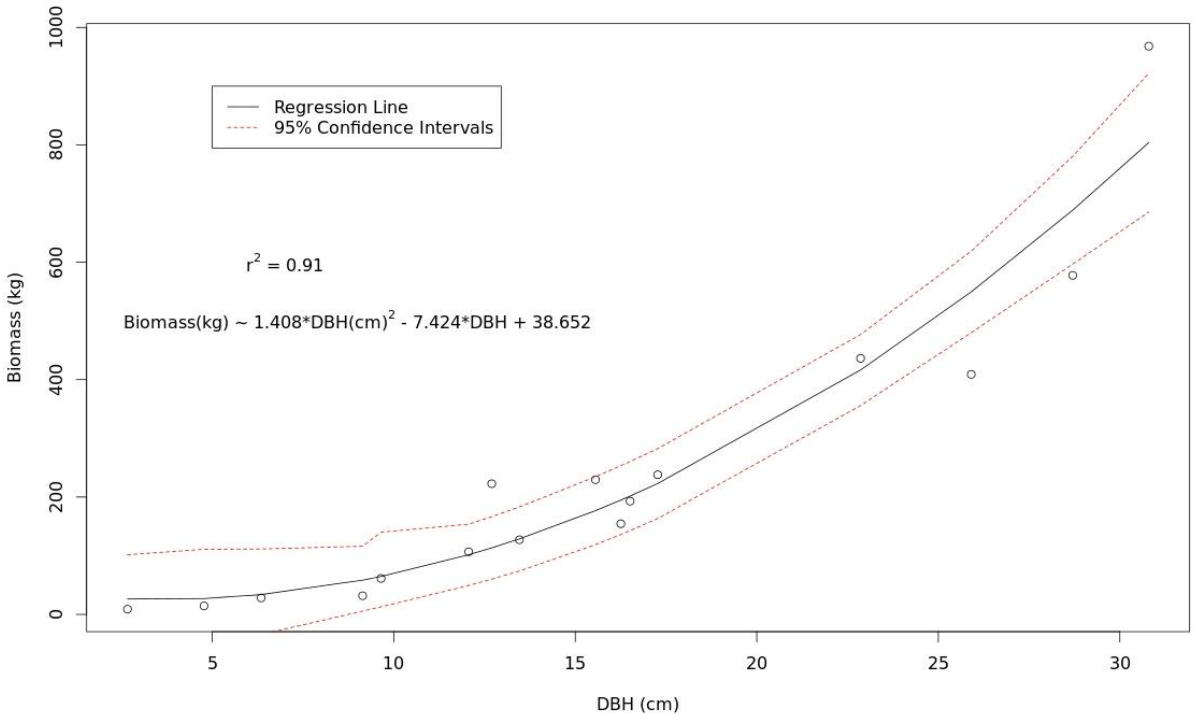

Figure 3-4 Allometric equation relating diameter at breast height (DBH) to biomass developed using data collected at our study sites as well as data from the NRES capstone course the year prior.

Table 3-1 Summary of site measurements for each ground reference plot.

Site	Average Age	Max Age	LiDAR Derived Canopy Height (m)	Ground Mean Tree Height (m)	Percent Cover Derived From Imagery	Densiometer Cover	Biomass (kg)
1	34.6	45	6.096	8.33	81.43%	92.24%	4992.73
2	30.25	40	2.902	7.70	46.94%	61.10%	2936.36
3	37	48	4.032	7.97	80.89%	81.44%	5288.64
4	29	43	2.76	7.91	50.00%	37.28%	3506.36
5	24	28	1.939	4.73	59.18%	42.22%	1595.00
6	N/A	N/A	4.335	8.42	79.59%	99.32%	3492.73
7	N/A	N/A	3.712	7.71	78.57%	86.84%	6008.64
8	N/A	N/A	4.112	7.45	53.57%	98.28%	5667.27
9	N/A	N/A	1.828	7.23	48.47%	61.20%	1955.91
10	N/A	N/A	0.911	4.61	16.84%	11.13%	686.82
11	N/A	N/A	0.919	4.05	17.86%	8.68%	410.45
12	N/A	N/A	2.063	6.24	47.96%	50.80%	2122.27
13	N/A	N/A	5.845	N/A	79.59%	89.39%	6467.73
14	N/A	N/A	2.669	5.60	54.08%	68.07%	2555.91
15	N/A	N/A	5.372	7.75	63.27%	75.30%	3670.00
16	N/A	N/A	1.1	4.42	11.73%	10.24%	395.91
17	N/A	N/A	1.699	4.76	22.45%	8.32%	859.09

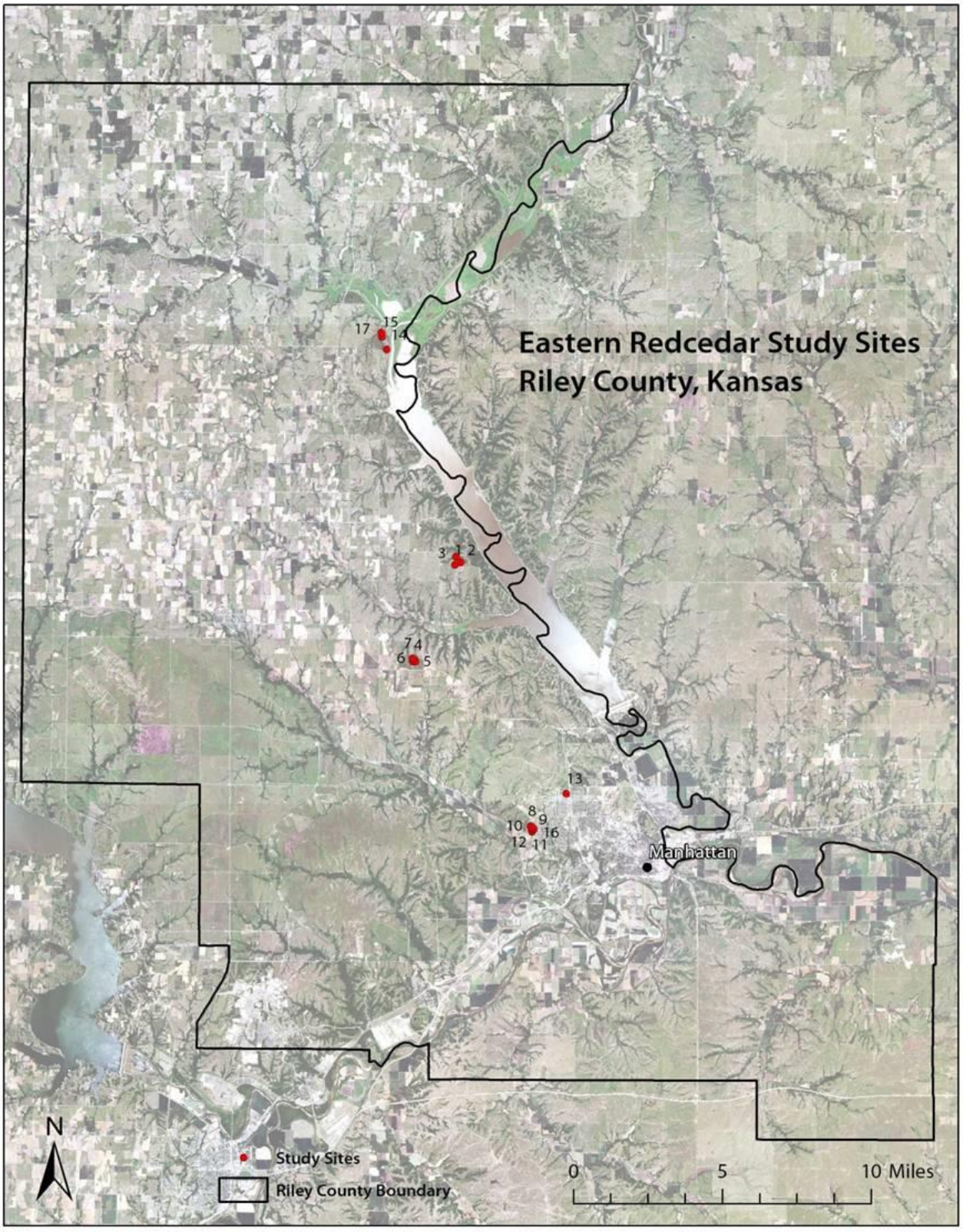

Figure 3-5 Map of Riley County, Kansas showing study plot locations in red.

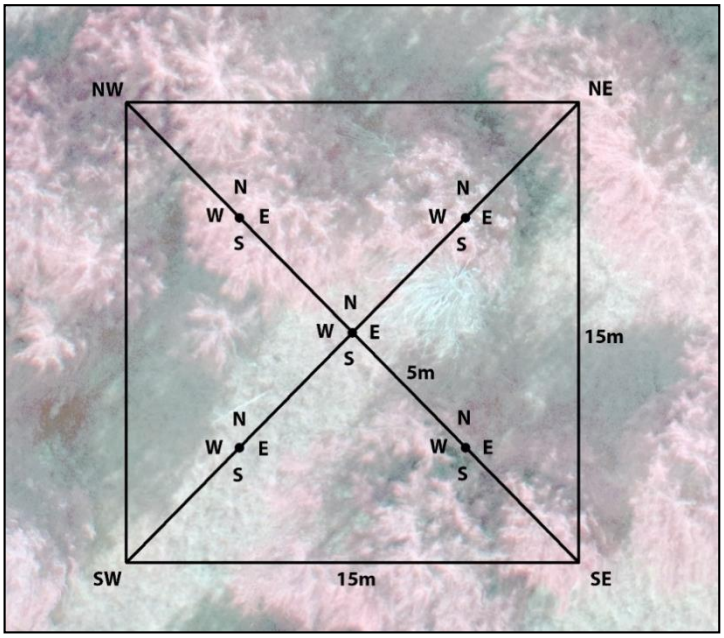

Figure 3-6 Aerial schematic of the modified point-center quarter sampling method at a study site.

3.2.3 LiDAR pre-processing

LiDAR data were obtained from the Kansas GIS Data Access Support Center (DASC) in .LAS format which contains the raw xyz coordinates of each point along with the return number. The dataset had been processed from its raw form which contains XYZ information along with sensor orientation, scan direction and range into LAS format projected in NAD 83 UTM Zone 15N by the vendor. Data were also classified into bare-earth returns versus all other returns by the distributer, however no further classification had been performed. Nominal point spacing was between 1.0 and 1.4 meters and vertical accuracy was approximately 18 centimeters. The LiDAR data were collected in spring of 2010.

LiDAR LAS files were processed using the Merrick® Advanced Remote Sensing software package (MARS®) provided to us for temporary use by Merrick Inc. The MARS® software has several different methods for raster interpolation from an LAS point cloud. (Merrick and Company, 2013) One method interpolates raster cell values from a triangulated representation of the point cloud generated as an intermediary. It was decided that this method was too computationally intensive and time consuming to be used. The other method uses a binning process to assign grid cell values from point values. When more than one value is

present the software allows the user to select whether to use a minimum, maximum, or average value. Gaps of less than 1-meter are then filled using a linear interpolation. Bare-earth and first-return rasters were created using this procedure, bare-earth returns were identified using the classification codes provided by the distributer, with the averaging option being selected for cells with multiple values. Both raster files were exported in the ESRI® grid format for import into ArcGIS®. Each was gridded at 1.0-meter per pixel resolution.

3.2.4 Classification of multispectral imagery

Two types of multispectral imagery were used to assess the range and density of redcedar. Initially, a coarse (30-meter spatial resolution) Landsat classification was used to identify areas of redcedar cover. This classification ensured that areas of significant closed-canopy redcedar cover would be identified. It also provided a means of delineating the areas to be classified within the higher resolution data. The second round of multispectral classification involved the hybrid use of U.S. Department of Agriculture National Agricultural Imagery Program (NAIP) 4-band (NIR-R-G-B) data and LiDAR. Within areas already identified as containing redcedar based on the coarser Landsat classification, a second classification was derived from the higher resolution NAIP data. This allowed for a more accurate estimate of redcedar density. The resulting 1.0-meter spatial resolution classification of redcedar was subsequently used to identify the target species in a 1-meter LiDAR-derived canopy height model.

3.2.4.1 Unsupervised classification of Landsat Imagery

A multi-temporal classification technique was performed using cloud-free Landsat TM images from January 5, 2011 and August 1, 2011, representing winter and summer dates, respectively. Six bands from each image (omitting the thermal band) were stacked using ERDAS Imagine© software. The resulting 12-band image (see Figure 3.7) was used as the input in the ISODATA unsupervised classifier tool in ERDAS Imagine. Output settings were set at 50 clusters with a confidence interval of 0.95. The resulting 50 spectral clusters were manually interpreted by comparing them with ground truth data and high-resolution NAIP imagery. A modified Anderson Level I classification scheme (Anderson, 1976) was to classify each cluster. The Level I "forest land" class was split into "deciduous forest land" and "evergreen forest land" as indicated in level 2 of the Anderson scheme. This separation was preferred since evergreen

forest in the study area is almost exclusively comprised of eastern redcedar, the target land cover type.

The clusters that were interpreted to include redcedar cover were identified and extracted using ISODATA. An iterative process known as "cluster busting" was used to further refine the redcedar classification (Jensen, 2005). During cluster busting, the analyst identifies the clusters that include or that are most spectrally similar to the target land cover type. All other clusters are masked out, and ISODATA is performed a second time. This process often finds "hidden" spectral information that can reveal other land cover types in the image that were not evident in the initial ISODATA classification. Multiple iterations of cluster busting are sometimes necessary to accurately extract a particular land cover type, as was the case in extracting redcedar cover. For this study, two iterations were necessary to separate redcedar from other cover types. After redcedar was accurately classified, the classification accuracy was assessed using a simple random sampling scheme to visually compare the classified Landsat pixels with high resolution NAIP imagery in which redcedar cover was more obvious.

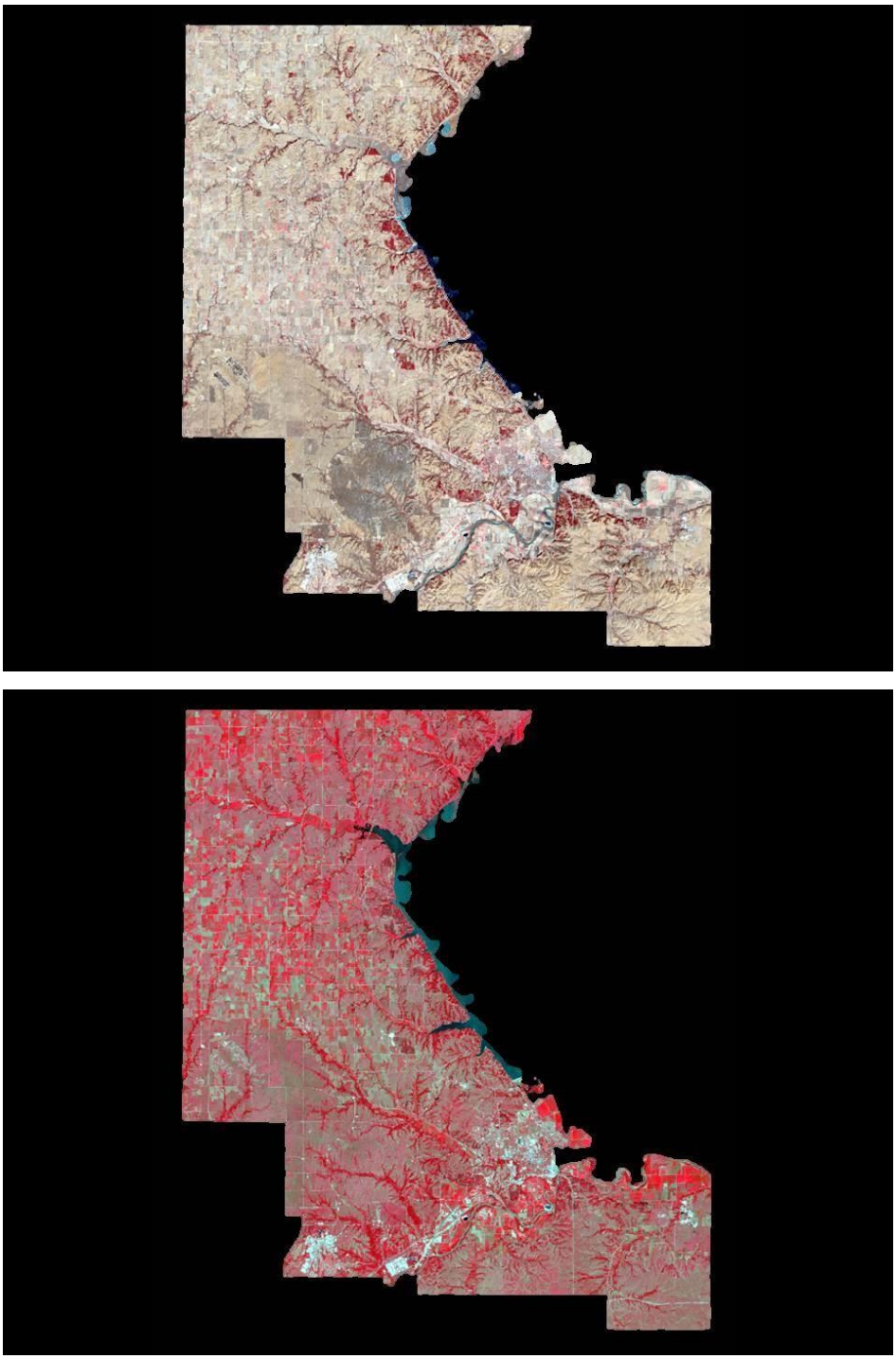

Figure 3-7 False-color composite (4-3-2) Landsat TM images of Riley County, Kansas from January 5, 2011 (top) and August 1, 2011 (bottom).

3.2.4.2 Classification of higher spatial resolution NAIP Imagery

USDA NAIP 4-band data from 2008 were obtained from the Kansas Data Access Support Center DASC. NAIP data were not available with a near-infrared band in the raw format for the same period as the LiDAR collection and therefore a decision was made to use the closest possible collection. The spatial resolution of the data was 1.0-meter and the data had been orthorectified. Multispectral data were co-registered to the LiDAR canopy models to ensure proper alignment (RMS error less than one pixel). Prior to classification of NAIP data, all areas within the imagery corresponding with areas in the canopy height model below 0.5 meters were masked out. This removed any remaining water pixels and shadow on the ground, both of which were easily confused with dark shadowed redcedar spectral values in the data. An unsupervised classification was then conducted for all areas classified as redcedar in the initial Landsat classification.

Once again, the ISODATA classification algorithm was used to produce 50 clusters. Clusters were visually interpreted and assigned to redcedar and non-redcedar classes. User's accuracy was calculated using 100 randomly selected validation samples, which were evaluated using a combination of site survey and imagery interpretation. Percent cover by redcedar was calculated from the classified NAIP data for each of the 17 study sites using the ArcGIS® zonal statistics tool.

3.2.5 Redcedar canopy model development

Development of a biomass prediction model for redcedar first necessitated the removal of other aboveground structures and tree species from the canopy height raster. This was accomplished using a 1.0-meter resolution redcedar binary mask created from the classified image data. The application of this mask resulted in a canopy height model representative of only redcedar canopy height.

The ArcGIS® zonal statistics tool was used to calculate the following summary statistics of the canopy height model for each of the 17 study sites: sum of canopy height, mean canopy height, median canopy height, maximum canopy height, minimum canopy height, and standard deviation of canopy height. Zeros were not included in the calculation of zonal statistics pertaining to the canopy height model. The exclusion of zeros allowed for the calculation of a more accurate measure of mean canopy height.

3.2.6 Biomass predictive model and map development

Development of a predictive statistical model for biomass began with the extraction of metrics for each sample plot from both the canopy height model and the redcedar classification. These metrics included: percent cover by redcedar derived from the high-resolution NAIP classification map, sum of canopy height, mean canopy height, median canopy height, maximum canopy height, minimum canopy height, and standard deviation of canopy height. Stepwise linear ordinary least squares regression was used to determine the most accurate model for biomass prediction using these parameters. Models were evaluated on Root Mean Squared Error, Bayesian information criterion, and coefficient of determination.

After a predictive equation was developed, a map of redcedar biomass was calculated using ArcGIS® spatial modeler. First, the ArcGIS® block statistics tool was used to calculate percent cover of redcedar within a 15x15 meter window. The same procedure was also used to calculate mean canopy height within a 15 x15 meter window. A weighted overlay was then used to calculate a 15-meter resolution biomass raster. The resulting map was resampled to 30-meter and 60-meter resolution in both short (imperial) tons and metric tons for dissemination to interested parties.

3.3 Results

3.3.1 Redcedar Canopy Model

Figure 3.4 shows the resulting equation relating diameter at breast height (DBH) to tree biomass. This equation was used to calculate biomass for each ground control site. Statistics include average tree age, maximum tree age, and mean tree height of selected trees as well as percent cover by redcedar (calculated from densiometer readings) and biomass (calculated as a sum of tree biomass for each site derived from diameter at breast height and the allometric equation).

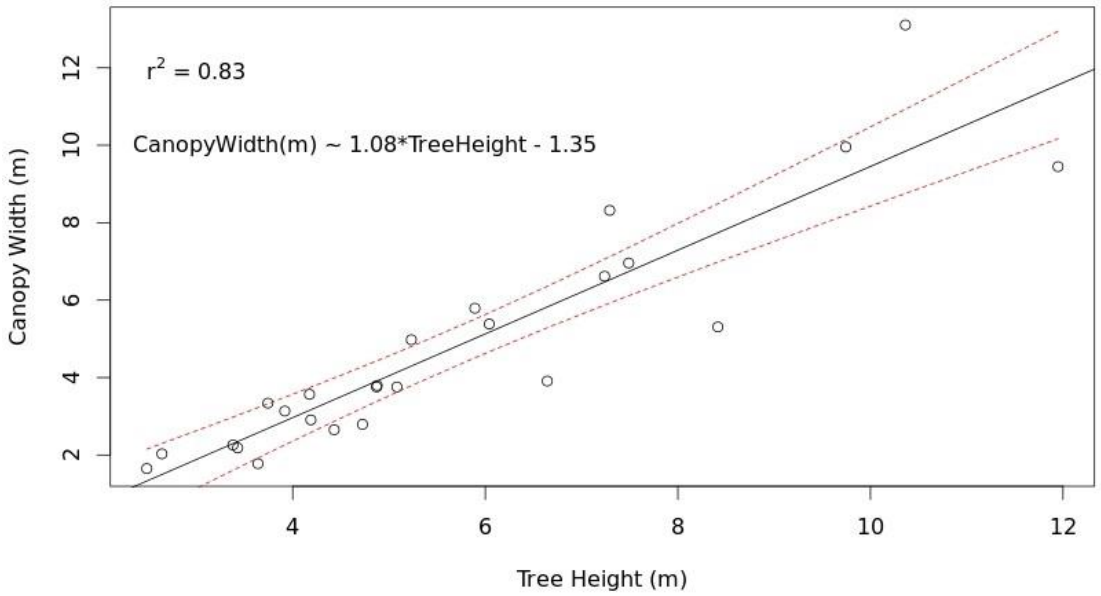

Figure 3-8 Allometric equation, developed from field data collected at our study sites, relating redcedar canopy width to tree height.

The relationship between the plot-level mean height of the redcedar canopy height model based on LiDAR data and the mean tree height of selected trees in ground reference plots can be seen in the graph in Figure 3.8. The model is precise ($r^2 = 0.77$, $p \leq 0.05$) however there is considerable bias y-intercept > 4 meters. The Root Mean Squared Error of the model was calculated to be 0.74 meters. While a bias is present and some error exists the precision of this relationship suggests that LiDAR be used to model redcedar canopy height if the bias is considered. There was a strong relationship ($r^2 = 0.81$, $P = 0.05$) between the percentage of redcedar cover as calculated from the classified NAIP data and the percentage estimated on the ground using densiometer readings (Figure 3.9).

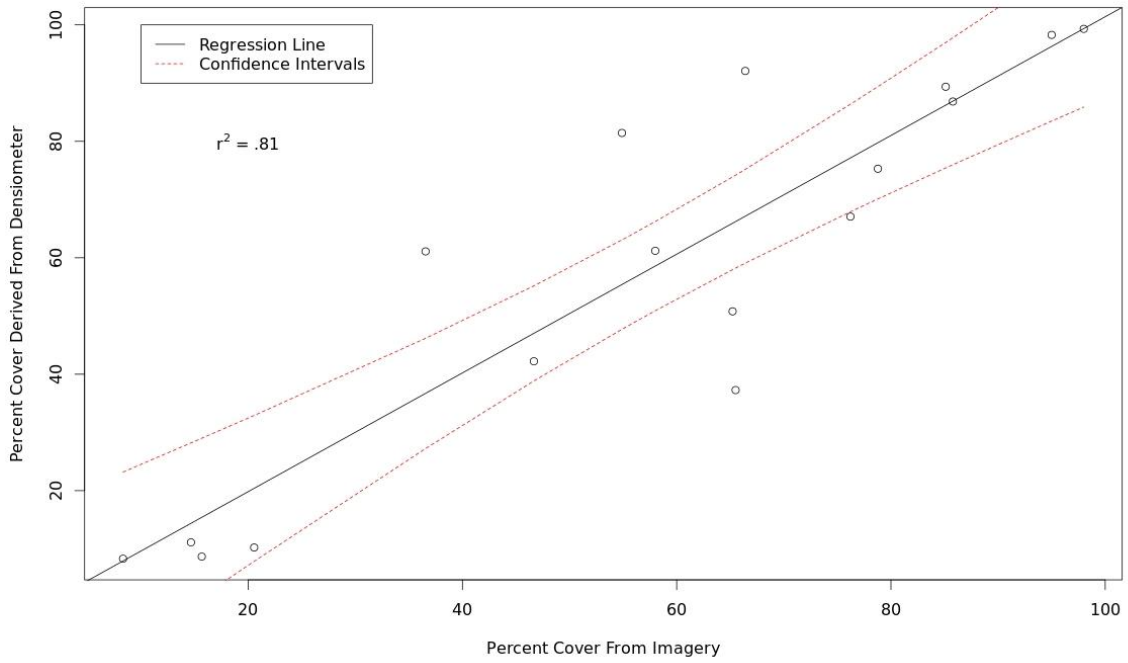

Figure 3-8 Aerial percent cover vs. ground canopy cover (measured with densiometer).

3.3.2 Biomass Predictive Model

Stepwise model selection using a forward and backward model selection with Akaike Information Criterion (AIC) as the selection criterion was used to identify the optimal LiDAR derived canopy height metric for prediction of biomass. Mean canopy height derived from LiDAR, and percent cover derived from classified imagery, were identified as the best predictors of redcedar biomass. This model also produced the lowest residual sum of squares and subsequently the lowest root mean square error (RSME).

Results of accuracy assessment of the final model are provided in Table 3.2. The final model was developed and tested in the Weka® data mining software and a jackknife approach (k-folds cross-validation) was used to test model accuracy due to the limited size of the dataset. The model's root-mean squared error calculated using the cross-validation approach was approximately 35 megagrams (metric tons) per hectare. It should be noted that the model shows a considerable bias in the model with a y-intercept of –676 Megagrams/hectare. The model was produced using LiDAR mean height values ranging from 0.91 meters to 7 meters and percent

cover values from 11% to 81%. Values outside this range for either metric may produce unreliable or problematic results.

Table 3-2 Accuracy assessment summary of the redcedar biomass prediction model. Showing Biomass as a function of Percent Cover and Mean Canopy Height

Equation	R-Squared	Root Mean Square Error	P-Value
Biomass = 3655.48 * Percent Cover + 602.02 * Mean Canopy Height - 676.03	0.72	35 Megagrams/Hectare or 792 kg/ 225 square meter Plot	< 0.05

3.4 Discussion and Conclusions

The combined use of LiDAR and multispectral remotely sensed data was again shown to be an effective method of assessing the biomass of a target species within a heterogeneous landscape. It is therefore well-suited for monitoring the encroachment of undesirable woody species. Model error, as measured by root mean square error, was within the range of previous models using LiDAR data to predict biomass (Drake *et al.*, 2003).

3.4.1 Sources of Error

A possible source of error includes the incongruence between the dates of collection for remotely sensed and ground reference data. Another potential source of error is the coarse point spacing of the LiDAR which is approximately 1-meter, a denser point spacing could result in a more detailed model of redcedar canopy and therefore a better estimation of biomass. The vertical accuracy of the LiDAR should also be considered; vertical accuracy was stated by the vendor to be approximately +/- 0.18 meters which could account for some inaccuracy in the model. The propagation of errors associated with the remotely sensed data along with any errors in the DBH biomass model, used as a proxy for in-situ biomass measurements, could all contribute to the overall accuracy of the final model.

Even given these sources of error it should be noted that the Root Mean Square Error for the model of 35 Megagrams/hectare was in line with previous studies using LiDAR to model tree biomass (Drake *et al.*, 2003).

3.4.2 Future Work

Future work includes expanding the study to other areas prone to redcedar encroachment, improving model accuracy by simultaneous collection of ground reference and remotely sensed data, and exploration of other LiDAR-based forest inventory techniques such as individual tree extraction. Tighter LiDAR point spacing could allow for better characterization of crown shape and for the use of individual tree-based approaches.

Based upon the findings of this study it is feasible for the biofuels industry to use a hybrid approach of imagery classification and LiDAR canopy height classification in areas where these data are available to identify landscapes of sufficient redcedar biomass for harvest and processing as biofuel. There is however always room for improvement, future studies should be conducted to determine if higher density LiDAR data could improve model accuracy.

References

1. Anderson, J. R., E. E. Hardy, J. T. Roach, and R. E. Witmer. 1976. *A Land Use and Land Cover Classification System for Use with Remote Sensor Data*. Washington, D.C.: United States Government Printing Office.

2. Briggs, J. M., and D.J. Gibson. 1992. "Effect of Burning on Tree Spatial Patterns in a Tallgrass Prairie Landscape." *Bulletin of the Torrey Botanical Club* 119: 300–307.

3. Briggs, J. M., G. A. Hoch, and L. C. Johnson. 2002. "Assessing the Rate, Mechanisms, and Consequences of the Conversion of Tallgrass Prairie to Juniperus Virginiana Forest." *Ecosystems*. 5 (6): 578–586.

4. Briggs, J. M., A. K. Knapp, and B. L. Brock. 2002. "Expansion of Woody Plants in Tallgrass Prairie: A Fifteen-Year Study of Fire and Fire-Grazing Interactions." *American Midland Naturalist* 147 (2): 287–294.
URL: http://www.jstor.org/stable/3083203.

5. Bortolot, Z. J., and R. H. Wynne. 2005. "Estimating Forest Biomass Using Small Footprint LiDAR Data: an Individual Tree-Based Approach That Incorporates Training Data." *ISPRS Journal of Photogrammetry and Remote Sensing* 59 (6): 342–360.

6. Coppedge, B. R., D. M. Engle, R. E. Masters, and M. S. Gregory. (2001). "Avian Response to Landscape Change in Fragmented Southern Great Plains Grasslands." *Ecological Applications* 11 (1): 47–59.

7. Chapman, R. N., D. M. Engle, R. E. Masters, and D. M. Leslie Jr. (2004) "Tree Invasion Constrains the Influence of Herbaceous Structure in Grassland Bird Habitats." *Ecoscience* 11 (1): 56–63.

8. Drake, J. B., R. G. Knox, R. O. Dubayah, D. B. Clark, R. Condit, J. B. Blair, And M. Hofton. (2003). "Above-Ground Biomass Estimation in Closed Canopy Neotropical Forests Using Lidar Remote Sensing: Factors Affecting the Generality of Relationships." *Global Ecology and Biogeography* 12 (2): 147–159.

9. Goesele, Michael, Noah Snavely, Brian Curless, Hugues Hoppe, and Steven M. Seitz. "Multi-view stereo for community photo collections." In 2007 IEEE 11th International Conference on Computer Vision, IEEE, 2007. pp. 1-8.

10. Horncastle, V. J., E. C. Hellgren, P. M. Mayer, A. C. Ganguli, D. M. Engle, And D. M. Leslie Jr. (2005) "Implications of Invasion by Juniperus Virginiana on Small Mammals in The Southern Great Plains." *Journal of Mammalogy* 86 (6): 1144–1155.

11. Jensen, J. R. 2005. *Introductory Digital Image Processing: A Remote Sensing Perspective*. Upper Saddle River: Pearson Prentice Hall.

12. Lucas, R. M., N. Cronin, A. Lee, M. Moghaddam, C. Witte, and P. Tickle. (2006). "Empirical Relationships between AIRSAR Backscatter and Lidar-Derived Forest Biomass, Queensland, Australia." *Remote Sensing of Environment* 100 (3):407–425.

13. Norris, M., J. Blair, L. Johnson, and R. Mckane. (2001). "Assessing Changes in Biomass, Productivity, and C and N Stores Following Juniperus Virginiana Forest Expansion into Tallgrass Prairie" Canadian Journal of Forest Research 31: 1940–1946.

14. Owensby, C. E., K. R. Blan, B. J. Eaton, and O. G. Russ. 1973. "Evaluation of Eastern Redcedar Infestations in the Northern Kansas Flint Hills." *Journal of Range Management* 26 (4): 256–260. URL: http://www.jstor.org/stable/3896570.

15. Popescu, S. C., and R. Wynne. (2004a). "Seeing the Trees in The Forest: Using Lidar and Multispectral Data Fusion with Local Filtering and Variable Window Size for Estimating Tree Height." *Photogrammetric Engineering and Remote Sensing* 70 (5):589-604.

16. Popescu, S. C., R. H. Wynne, and J. A. Scrivani. (2004b). "Fusion of Small-Footprint Lidar and Multispectral Data to Estimate Plot-Level Volume and Biomass in Deciduous and Pine Forests in Virginia, USA." *Forest Science* 50 (4): 551–565.

17. Slusher, J.P. (1995). "Wood Fuel for Heating." In University of Missouri Extension. URL: http://Extension.Missouri.Edu/Publications/Displaypub.Aspx?P=G5450

18. Starks, P. J., B. C. Venuto, J. A. Eckroat, and T. Lucas. (2011). "Measuring Eastern Red Cedar Juniperus Virginiana L. Mass with the Use of Satellite Imagery." *Rangeland Ecology & Management* 64 (2):178–186.

19. Stipe, D. J., and T. B. Bragg. (1989). "Effect of Eastern Red Cedar on Seedling Establishment of Prairie Plants." *Proceedings of the Eleventh North American Prairie Conference. 101–102*

20. Swatantran, A., R. Dubayah, D. Roberts, M. Hofton, and J. B. Blair. (2011). "Mapping Biomass and Stress in The Sierra Nevada Using Lidar and Hyperspectral Data Fusion." *Remote Sensing of Environment* 115 (11): 2917–2930.

21. Triggs, Bill, Philip F. McLauchlan, Richard I. Hartley, and Andrew W. Fitzgibbon. "Bundle adjustment—a modern synthesis." In *Vision algorithms: theory and practice*, pp. 298-372. Springer Berlin Heidelberg, 1999.

22. Wylie, B. K., D. J. Meyer, M. J. Choate, L. Vierling, P. K. Kozak, And R. O. Green. (2000). "Mapping Woody Vegetation and Eastern Red Cedar in The Nebraska Sand Hills Using AVIRIS." Paper Read at AVIRIS Airborne Geoscience Workshop. JPL Publication 00-18. Pasadena, CA Jet Propulsion Laboratory, California Institute of Technology

Chapter 4 - Exploring New Potential for the Use of Structure-from-Motion Photogrammetry as an Alternative to LiDAR for Modeling of Redcedar Canopy Height.

4.1 Introduction

For over 50 years, the invasion of woody plant species into rangelands throughout the tallgrass prairie ecoregion has been a serious concern to ranchers and conservationists (Owensby, *et al.*, 1973). Among the most prominent of these species is *Juniperus virginiana* L., often called eastern redcedar (Owensby, *et al.*, 1973; Norris, *et al.*, 2001) (Figure 3.1). Eastern redcedar has a large range encompassing most of the eastern United States. (Norris, *et al.*, 2001) The species is fast-growing, and birds can transport its seeds over many miles (Briggs, *et al.*, 2002). Historically, prior to the widespread suppression of natural prairie fires in the region, periodic burning of the prairie prevented eastern redcedar overexpansion (Briggs and Gibson, 1992; Briggs, *et al.*, 2002). Anthropogenic fire suppression has now resulted in the drastic expansion of its range (Strine, 2004; Owensby, *et al.*, 1973). In much of the Great Plains, this expansion has become an economic threat to the cattle ranching industry due to the loss of rangeland available for cattle grazing (Schmidt, 2002). Along with economic impacts caused by redcedar expansion, there are also environmental impacts, including losses in plant and animal community diversity and increased soil erosion (Chapman, 2004; Horncastle, 2005; Briggs, *et al.*, 2002). Closed-canopy redcedar forests also present a wildfire danger where redcedar expansion occurs near urban areas (Ward, 2013).

A potential solution to the problem of redcedar invasion is to find a large-scale commercial use for redcedar biomass. Since eastern redcedar is a plentiful species that is "out of place" (Blatchley, 1912) in the prairie ecosystem, there has been interest in harvesting redcedar stands for a variety of uses. Traditionally, redcedar wood has been used in fence posts and furniture, and it is commonly turned into mulch for gardening use. The wood can also be chipped and burned in wood-burning stoves or boilers, and methods are being developed to convert redcedar material into liquid biofuel products (Hemmerly, 1970; Lam, 2012; Ramachandriya, *et al.*, 2013). Redcedar oil has also been utilized in the essential oil industry and reportedly has

antibacterial and anti-cancer properties (Gawde, *et al.*, 2009; CAFNRnews, 2008; Semen & Hiziroglu, 2005).

Before redcedar can be harvested for use as a biofuel or other product, it must be determined if there is enough redcedar biomass in an area to allow a harvesting industry to be economically viable in that area, especially considering the costs of transporting the trees from harvest locations to a refinery. For harvesting to be cost-effective, it is best that large numbers of trees be clustered tightly together within an economically sustainable distance of processing facilities. While estimates of the overall scope of redcedar invasion and general estimates of biomass exist (Grabow and Price, 2010; Moser, *et al.*, 2008), there is little information on the spatial distribution of this biomass within Kansas. Currently available redcedar biomass information, collected using a random ground sampling technique (Bechtold & Patterson, 2005), has been shown in many cases to be inaccurate at a county level.

Considering eastern redcedar's detrimental environmental and economic impacts, as well as its potential commercial benefits it is necessary to establish cost-effective methods to map its extent and biomass distribution. This chapter explores the potential for Structure from Motion (SfM) photogrammetry as an alternative to LiDAR for mapping redcedar height in order to determine whether the method is a feasible alternative. Sense structure from motion photogrammetry requires less expensive hardware than LiDAR to obtain data it could be a viable alternative in some circumstances.

4.1.1 Structure from Motion Photogrammetry

In recent years, a new methodology for collecting three-dimensional data over large areas has become more widely available. Originating from the computer vision community in the 1990s, Structure-from-Motion or SfM photogrammetry differs from a traditional photogrammetric approach in that the technology allows for the automated extraction of the 3D coordinates of objects without the need for manual input of tie points. This is accomplished through the automated extraction of features within multiple overlapping images followed by the application of and iterative bundle adjustment procedure (Snavely, 2008). The capabilities of this technique were demonstrated by the application of structure from motion techniques to overlapping photos downloaded from community websites to produce three dimensional models of well-known world architectural sites (Goesele, 2007). More recently the technology has widely been used

with aerial imagery collected from Unmanned Aerial Vehicles (UAVs) for the construction of high resolution, high accuracy three dimensional models. In a study conducted on coastal erosion using SfM an accuracy of 25-40 mm was achieved using a multi-rotor UAV flying at 40 meters above ground level at low speed (Harwin and Lucieer, 2012). With the advent of commercial software packages such as Agisoft® PhotoScan and Pix4D® Mapper and the increased prevalence of greater computing power at a decreased cost Structure from Motion has now become easily accessible and will open up many opportunities for the generation of three-dimensional data at lower costs.

4.1.1.1 Structure from Motion Workflow

The SfM workflow consists of data collection, SfM processing, and post processing. For the data acquisition step images are acquired using a traditional metric camera or consumer grade camera from either a manned aircraft or a Small Unmanned Aerial System. For measurement and correct geo-referencing of the resulting data to be possible without considerable ground control the GPS location of the camera when the image was taken is recorded in the photo metadata through a process called geo-tagging. (Figure 4.1). Ground control points or reference measurements may optionally be collected for additional correction of scale and position of the resulting dataset.

Feature extraction can be accomplished using several algorithms with one of the most popular being the SiftGPU algorithm described in which has been shown to generate a robust set of feature descriptors for image features extracted from different viewing angles (Lowe, 1999). Following identification of individual image features the features are then matched between images based upon distinct feature characteristics. For the purposes of SfM features much be matched within a minimum of three images to be held as a keypoint. Through the triangulation of matched keypoints image orientation and three-dimensional positon of image points can be calculated. This is followed by an iterative bundle adjustment process which further optimizes the calculation of image positon (Triggs *et al.*, 2000). At this point any geolocation or orientation information collected with the images can be used for further calibration of the model. This process results in a sparse point cloud which contains points representing the 3D coordinates of the matched image features (Figure 4.3). At this point the density of the sparse point cloud may optionally be increased using one of several dense two-frame stereo correspondence algorithms, which take advantage of redundant information among individual image frames, may be used to

reconstruct the 3D geometry of areas between matched features that may be texture-less or occluded (D. Scharstein and R. Szeliski, 2002). Both the sparse and dense point clouds can be colorized using the original pixel values from the individual images or based upon relative or absolute elevation values for visualization (Figure 4.4). Finally, a digital elevation model (DEM) can be generated from the point cloud by the construction of a triangulated irregular network (TIN) or interpolation. Orthoimagery can then generated by mosaicking of the original images after they are orthorectified to correct for geometric distortions due to camera lens geometry, camera look angle and topographic relief. These factors can be calculated using the data generated during the bundle adjustment step of the SfM process along with the 3D surface model generated from the SfM point cloud (Figure 4.5).

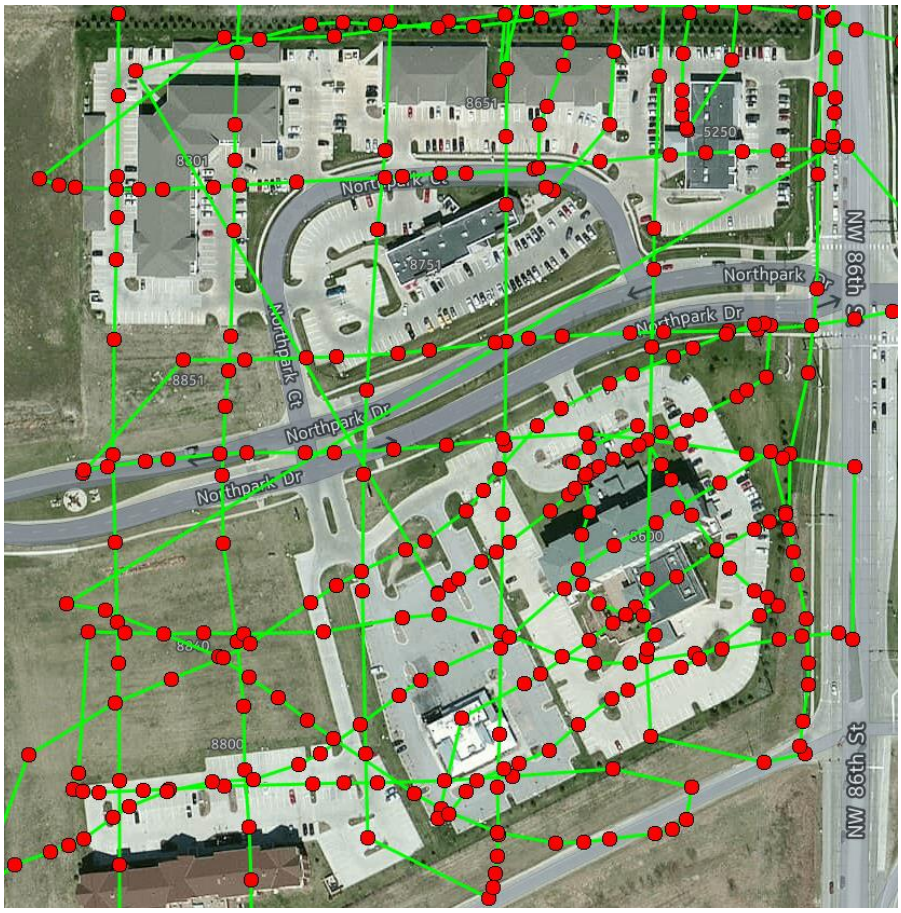

Figure 4-1 Geographic locations of individual photos overlaid on a web map.

During SfM processing keypoints are extracted through identification of unique features in individual images that can be used to determine image correspondence (Westoby, 2012) (Figure 4.2).

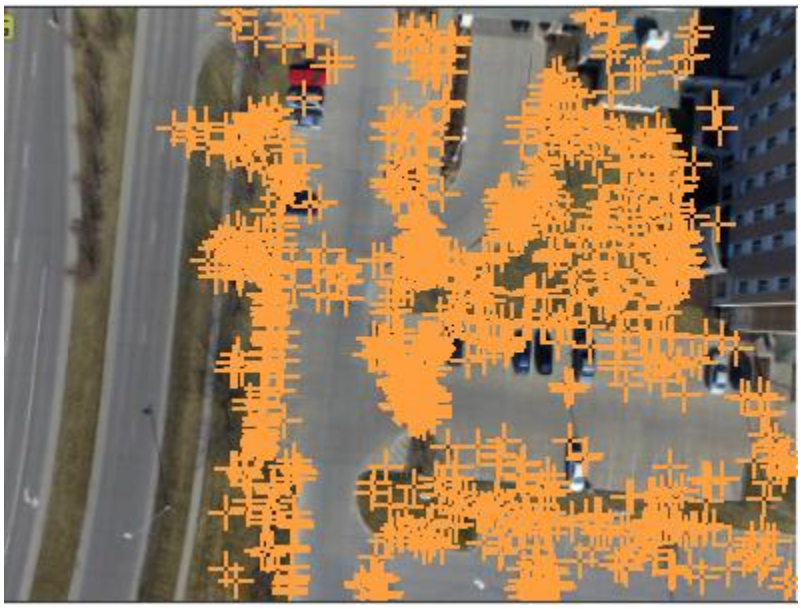

Figure 4-2 Locations of keypoints extracted from an image displayed as orange markers (Pix4d Mapper).

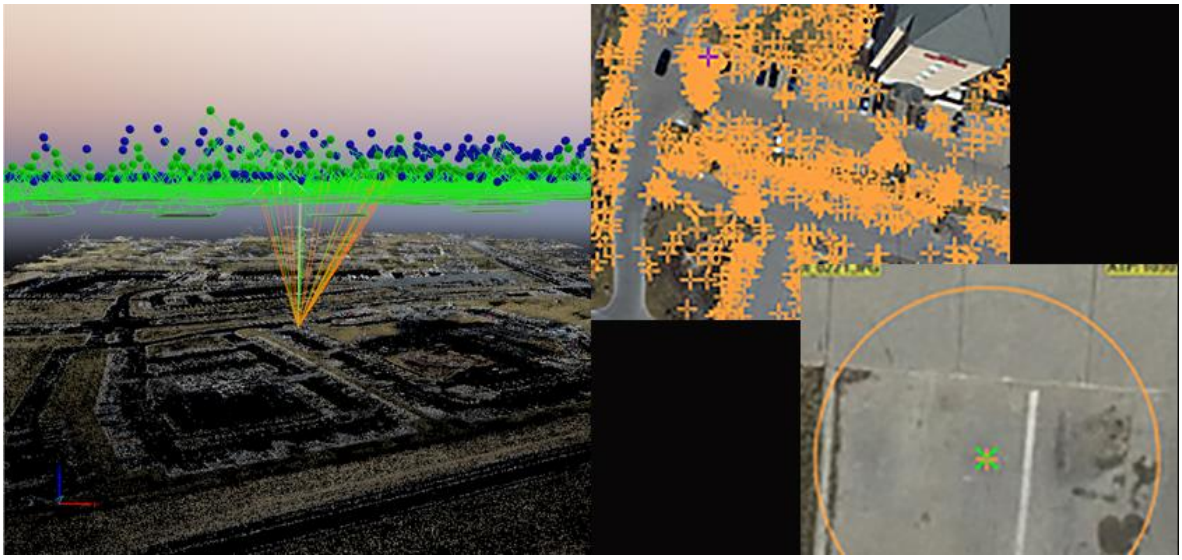

Figure 4-3 Individual image keypoint marked by a purple marker (top right) and vectors triangulating its 3D position from multiple images (left). The estimated accuracy of its 3D position is displayed as a circle around the marker in the bottom right image (Pix4D Mapper).

Figure 4-4 Dense point cloud.

Figure 4-5 TIN mesh surface generated from the point cloud and colorized using image values (top) and planimetrically corrected orthophoto overlaid on Mapbox basemap imagery to show georegistration.

.

4.1.1.2 Structure from Motion as an Alternative to LiDAR

Until recently the computational intensity of the SfM process meant that the technology was limited to very small areas. Recent advances in computer processing capabilities and improvements to algorithms has begun to change this (Westoby, 2012).

SfM has been shown to compare to LiDAR in the ability of the technology to produce three-dimensional data products. Research by Westoby and Brasington (2012) found that a digital elevation model (DEM) produced from SfM compared to the decimeter scale vertical accuracy of terrestrial LiDAR over a range of complex topographies and cover types. In 2013 Fritz reported a "promising potential for UAV-based 3D-reconstruction of forest stands" using SfM photogrammetry (Fritz, 2013).

One of the major benefits of Structure from Motion technology when compared to LiDAR is the relative cost of collecting data. LiDAR sensors often run in the range of $250,000 and up when taking all necessary components into account. Most require expensive twin-engine aircraft or helicopters to carry the sensor. Structure from motion data on the other hand can be collected using a variety of off-the-shelf cameras from small unmanned aircraft that can be bought for $1000 or small manned aircraft which are much less expensive than their larger twin-engine counterparts.

Given these new developments and the knowledge that an SfM based estimation of redcedar height would be much cheaper than using LiDAR I decided that an exploratory study be conducted to determine the feasibility for using SfM technology to measure the height of redcedar. The objective of this study was to compare height models generated using SfM to those produced using locally available LiDAR and to determine if accuracies of data collected using SfM could approach those of LiDAR with respect to calculating tree height.

4.2 Methods

4.2.1 Study Area

The project study area, an approximately 16-hectare (40-acre) site in Johnston Iowa, was selected due the existence of a preexisting dataset collected by AgPixel LLC., and funded by GTG Companies for company proprietary purposes. Permission was obtained from GTG and AgPixel to use the dataset for this thesis research. The site presented an opportunity to analyze a

SfM dataset containing a variety of cover types including manmade structures, impervious surfaces, an open field, and various tree species including eastern redcedar (Figure 4.6).

Figure 4-6 Orthoimagery showing the study site overlaid on a Mapbox® basemap.

4.2.2 Aerial Imagery Collection

Imagery for the project were collected as part of a commercial operation by AgPixel LLC under their FAA Section 333 exemption in February of 2016. During flight preplanning it was determined that the site was outside of the restricted airspace around Des Moines International Airport and therefore an additional Certificate of Authorization from the Federal Aviation Administration was not necessary (Figure 4.7). A notice to airman was filed the day prior to the flight and a licensed pilot was present per the Section 333 requirements laid out by the Federal Aviation Administration.

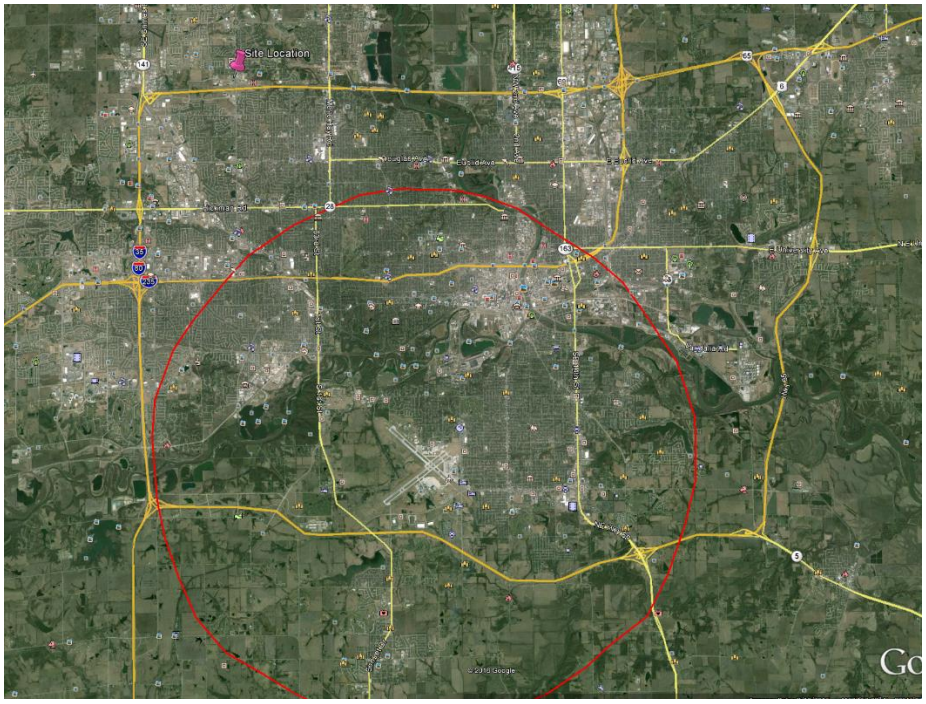

Figure 4-7 Map showing the study site (Fuchsia Pin) relative to the 5 mile no fly radius around the DSM airport (Red Circle).

4.2.3 Collection of in-situ ground-reference information

Ground control points were not collected due to the scope of the original project. An RTK GPS was not available to collect additional ground control so it was decided that several reference measurements be collected for data calibration and testing purposes. Time constraints, access to private property, and safety concerns working on public streets limited the number of these points. Permission could be obtained from the staff of the Hilton hotel on the site to collect measurements so all measurements were taken on that property. Table 4.1 shows the ground reference measurements collected using a clinometer including the hotel, road, and three redcedar trees selected using an opportunistic random sampling method.

Table 4-1 Measurements of objects collected on the ground for testing and calibration purposes

Object and Dimension	Measurement (meters)
Hotel height	22.3
Road width	11.98
Redcedar 1 height	4.12
Redcedar 2 height	4.33
Redcedar 3 height	8.42

4.2.4 SfM Data Processing

The imagery was processed by AgPixel LLC. using Pix4D mapper and a proprietary, automated workflow to generate derivative products including colorized surface models, contrast enhanced orthoimagery, and a point cloud product converted to work with a web based viewing software that allows for direct measurement of area, distance, and height profiles within the point cloud. The use of the road width and hotel height was considered as a means of increasing the relative accuracy of the model using the capability of the Pix4D software to use a scale constraint to calibrate the model's scale. It was decided not to conduct this procedure due to the ground measurements of the hotel and road deviating from the measurements collected from the uncalibrated SfM model by less than one percent.

4.2.5 Accuracy Assessment of the Model and Comparison to LiDAR Data

The SfM data were compared to LiDAR data collected in 2012 and accessed from the University of Northern Iowa's GeoTree data portal. The comparison consisted of a visual comparison of point cloud and digital surface model (DSM) data products as well as a regression analysis of data collected from the LiDAR and SfM DSM models at 2000 random points identified using the ArcGIS random points tool (Figure 4.8). It was determined that high spatial autocorrelation was likely among the random points and within the source data and therefore it was decided that this should be explored and accounted for in the comparison of the two datasets.

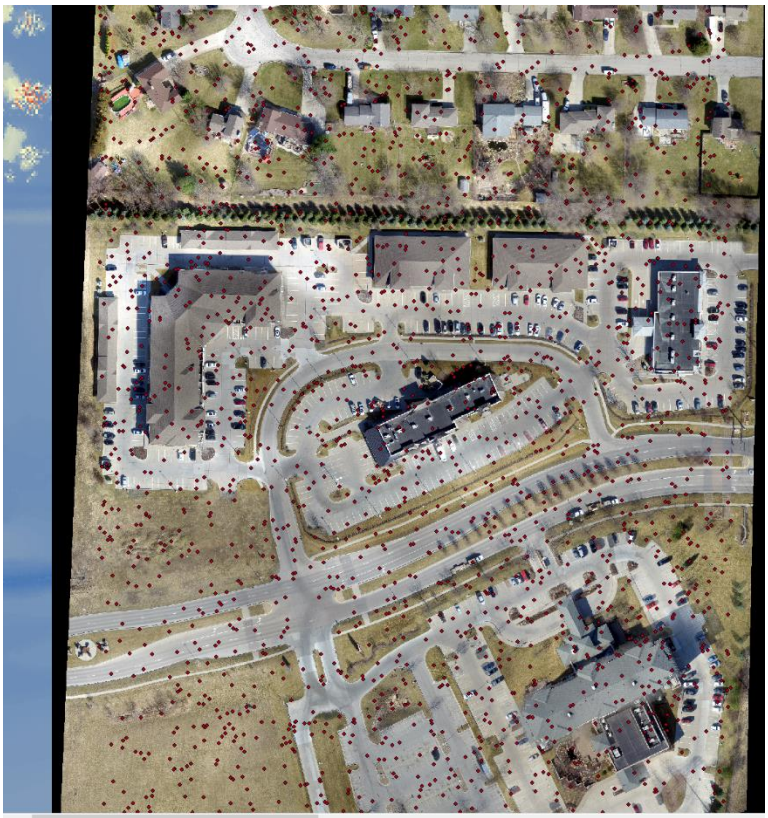

Figure 4-8 Random points for coinciding areas of LiDAR and SfM datasets.

Height and length measurements of multiple objects including redcedar trees, roadways, and buildings were extracted from the SfM point cloud using AgPixel's point cloud web viewer (Figure 4.9). The percent error was calculated for each object as well as the total Root Mean Square Error for both eastern redcedar trees and other objects including structure and roadways.

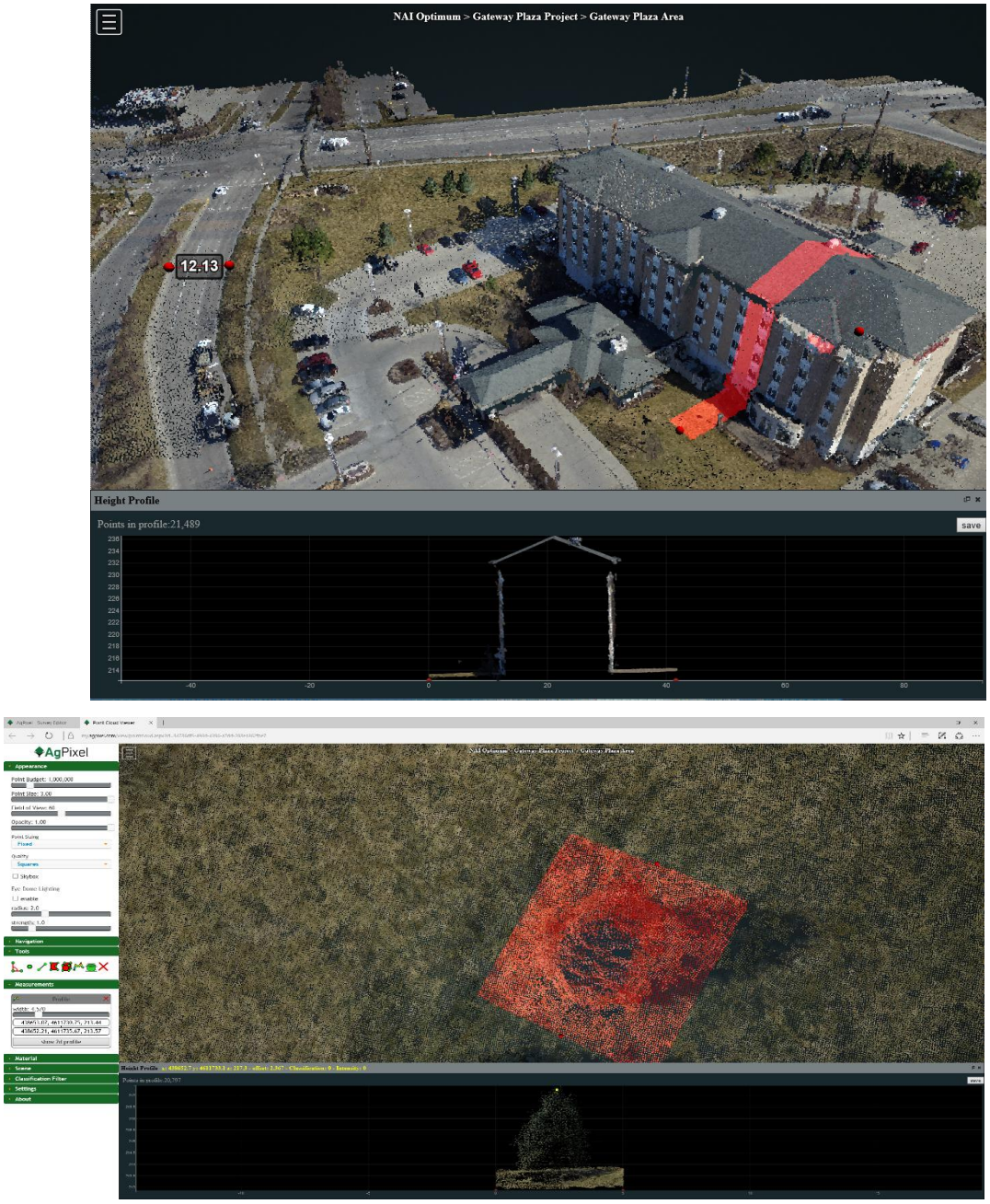

Figure 4-9 Images of AgPixel web point cloud analysis tool showing measurements for both the Hilton hotel (Top) and one of the eastern redcedar trees (Bottom).

4.3 Results

4.3.1 Comparison of SfM Data with LiDAR Data

Figure 4.10 shows a comparison of the LiDAR and SfM digital surface models at a location with three redcedar trees present. The LiDAR dataset was capable of producing a digital surface model with a ground sampling distance of 1.0-meter while the SfM dataset was processed at 10 centimeters. The native resolution of the SfM dataset was approximately 2 centimeters, but it was decided that the dataset be resampled to a coarser spatial resolution to minimize file size and processing time. The regression results of the two surface models can be seen in figure 4.11. The two datasets were shown to be correlated with an r-squared value of 0.76 and a p-value significantly below 0.05 (2.2e-16).

Given the nature of the sample points it was decided that the effects of spatial autocorrelation should be explored. The effects of spatial autocorrelation of the residuals were calculated using Moran's I and the residuals were found to be spatially auto correlated ($P << 0.05$). Variograms and spatial plots were also constructed to explore the spatial effect of residuals, but did not seem to indicate the same relationship. Figure 4.12 shows a spatial plot of residuals which seems to indicate little to no spatial autocorrelation with values showing a systematic and not repeating pattern. Figure 4.13 shows Semivariograms which indicate a pure nugget effect model in the 45 and 90 degree directions and a power law relationship in the 0 and 135 degree directions. These would tend to indicate no spatial autocorrelation and a complex scale-free relationship respectively.

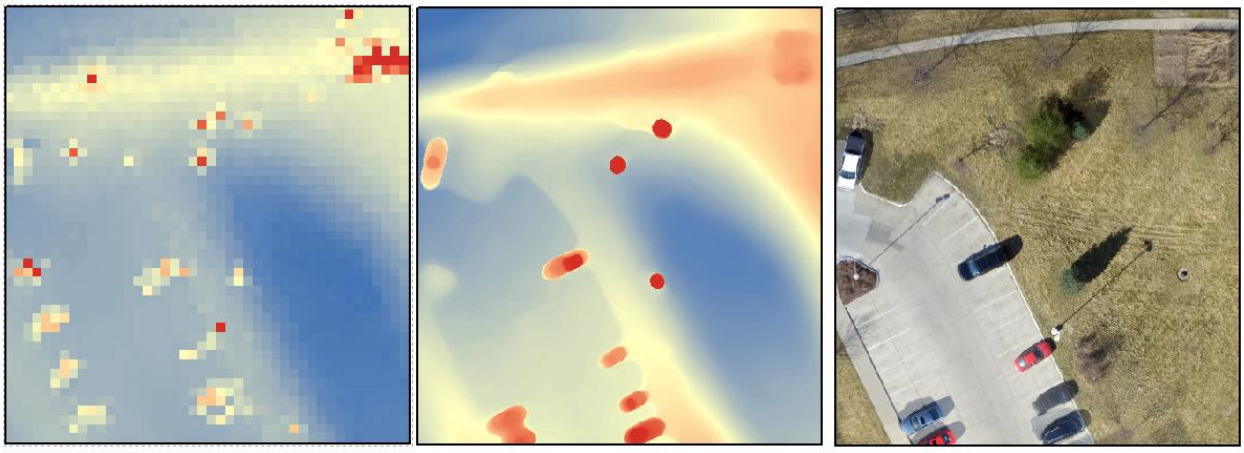

Figure 4-10 Comparison of LiDAR (Left) and SfM (Right) digital surface models in the same area with orthoimagery for reference (Right).

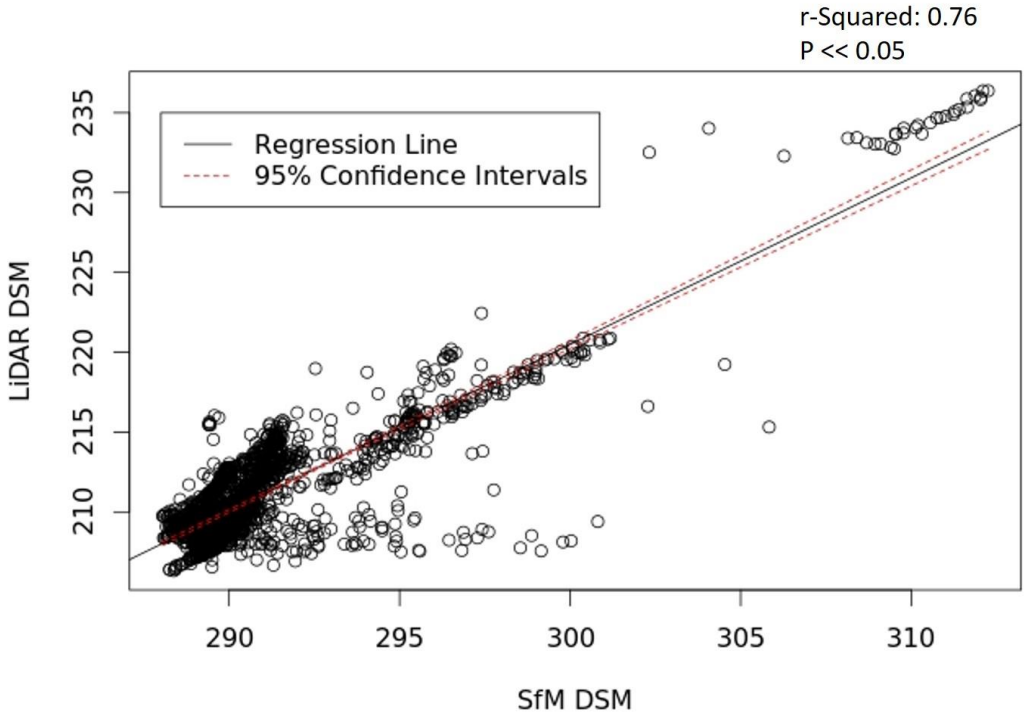

Figure 4-11 Graph showing the relationship between the SfM and LiDAR derived digital surface models (units in meters above sea level).

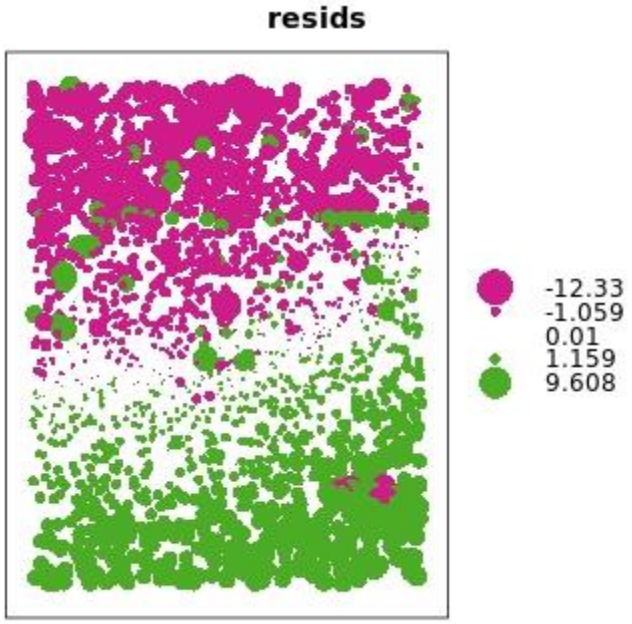

Figure 4-12 Spatial plot of residuals showing a strong effect of spatial autocorrelation.

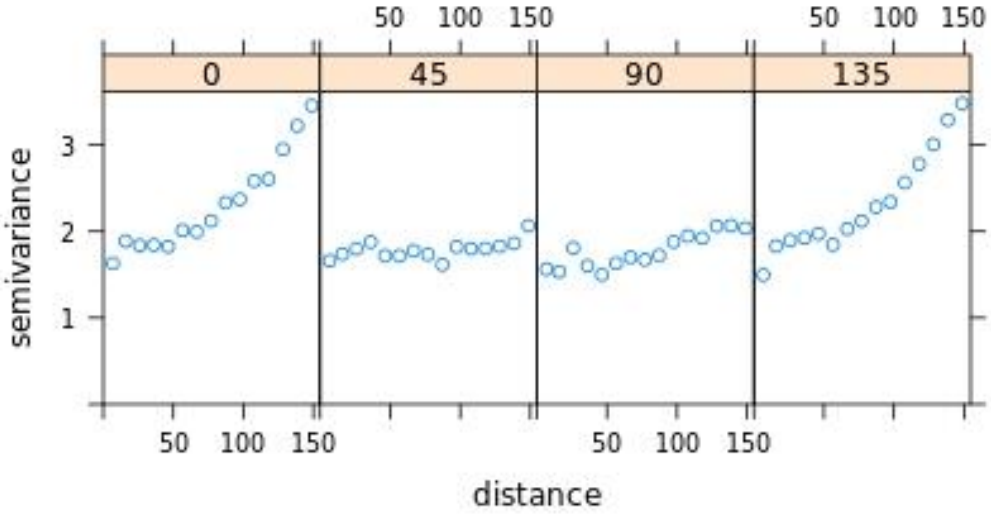

Figure 4-13 Semivariograms plot showing strong autocorrelation in N/S and SE directions

4.3.2 Comparison of SfM Derived Height Measurements with In-Situ Ground Measurements

A comparison of height and length dimensions extracted from the SfM point cloud using AgPixel's web based tool against the dimensions measured for those objects on the ground shows that there is a strong agreement between the two modeling methods. The root mean squared error for the tree height estimates was approximately 0.36 m and for all other objects was about 0.33 m. The percent of disagreement averaged around 6 percent for trees and 4 percent for all objects (Table 4.7). It was not possible to reliably extract individual measurements from the LiDAR surface for any objects other than the Hotel due to the coarse nature of the LiDAR dataset.

Table 4-2 Comparison of ground based height measurements and SfM height measurements with percent disagreement. Structure from motion +/- error estimated using the accepted error for SfM data stated by the software developer which is approximately 1-2 pixels without ground control.

Object	Ground (meters)	SfM (meters)	LiDAR (meters)	Disagreement with Ground (meters)	Disagreement with Ground (percent)
Road width	11.98	12.13 (+/- 4cm)		0.15	1.2
Hotel height	22.3	22.7 (+/- 4cm)	19.59 (+/- 0.18)	(SfM) 0.4 (LiDAR) 2.94	(SfM) 2.0 (LiDAR) 13.0
Lamp post Height	4.11	3.95 (+/- 4cm)		0.16	3.8
Redcedar 1 Height	4.12	3.9 (+/- 4cm)		-0.22	5.0
Redcedar 2 Height	4.33	4.9 (+/- 4cm)		0.57	13.0
Redcedar 3 Height	8.42	8.54 (+/- 4cm)		0.12	1.0
				RMSE Trees: 0.36 RMSE All: 0.33	

4.4 Discussion and Conclusions

4.4.1 Comparison of LiDAR and SfM

There was a correlation between the SfM and LiDAR models and the two showed a fair amount of visual similarity. There were several outliers in the model that could be due to differences in the collection dates of the LiDAR and SfM datasets and changes to the surface including construction, excavation, erosion and tree growth. There was of course a greater difference in the absolute difference in the elevations between the two models. This is likely due to the lack of RTK ground control points that would have increased the absolute accuracy of the SfM model although it is not unreasonable to assume some inaccuracy in the absolute values of the LiDAR dataset. A prior study by Javier in 2015 found that the absolute accuracy of be significantly improved using ground control and it is estimated to be possible to obtain a two-pixel absolute accuracy or better. When the spatial arrangement of objects in the two models was compared, it was clear that much greater detail could be seen in the SfM model due to higher spatial resolution of the SfM surface model. Collection of LiDAR with this resolution would be extremely expensive and cost prohibitive for an area of similar size to our study site. The increased spatial resolution of the SfM modeling technology enhances the potential for the success of automated tree canopy identification algorithms described in chapter two and greatly increases the possibility for direct manual measurement of objects within the point cloud. Collecting data for SfM for a drone over an area the size of a county is of course not practical and therefore a manned platform would need to be used. Future work needs to be done to determine if the accuracy of such a collection would compare favorably to LiDAR.

Given some of the inconsistencies in the analyses of spatial autocorrelation in the LiDAR to SfM comparison it may be prudent to explore this relationship further. Some factors affecting the spatial relationships might include the presence of relatively little topographic variation across the site and the presence of a large building and multiple small buildings. The presence of the large building may have something to do with the power law relationship seen in several of the variograms.

4.4.2 Accuracy Assessment of SfM Data Using Ground Control

The in-situ ground elevation measurements of object compared favorably with the measurements extracted from the SfM point cloud. It should be noted that the percent errors for the solid objects was generally lower than the percent error for the trees. This is likely due to the difficulty of precisely identifying the tree tops, both on the ground and in the 3D model, but could also be due to movement of the tree by wind during aerial data collection. It is worth mentioning the ease of use of the web-based profiling tool for extracting measurements from the point cloud. Such a tool could allow for easy measurement of trees within an area of interest. A RMSE of 0.36 meters is slightly higher than the estimated vertical accuracy of 0.18 meters for the LiDAR data used in previous chapters, but it should be noted that individual trees could not be consistently identified in that dataset. Introduction of RTK ground control has the potential to significantly improve this number.

References

1. Anderson, J. R., E. E. Hardy, J. T. Roach, and R. E. Witmer. 1976. *A Land Use and Land Cover Classification System for Use with Remote Sensor Data*. Washington, D.C.: United States Government Printing Office.

2. Briggs, J. M., and D.J. Gibson. 1992. "Effect of Burning on Tree Spatial Patterns in a Tallgrass Prairie Landscape." *Bulletin of the Torrey Botanical Club* 119: 300–307.

3. Briggs, J. M., G. A. Hoch, and L. C. Johnson. 2002. "Assessing the Rate, Mechanisms, and Consequences of the Conversion of Tallgrass Prairie to Juniperus Virginiana Forest." *Ecosystems*. 5 (6): 578–586.

4. Briggs, J. M., A. K. Knapp, and B. L. Brock. 2002. "Expansion of Woody Plants in Tallgrass Prairie: A Fifteen-Year Study of Fire and Fire-Grazing Interactions." *American Midland Naturalist* 147 (2): 287–294.
URL: http://www.jstor.org/stable/3083203.

5. Coppedge, B. R., D. M. Engle, R. E. Masters, and M. S. Gregory. (2001). "Avian Response to Landscape Change in Fragmented Southern Great Plains Grasslands." *Ecological Applications* 11 (1): 47–59.

6. Chapman, R. N., D. M. Engle, R. E. Masters, and D. M. Leslie Jr. (2004) "Tree Invasion Constrains the Influence of Herbaceous Structure in Grassland Bird Habitats." *Ecoscience* 11 (1): 56–63.

7. Drake, J. B., R. G. Knox, R. O. Dubayah, D. B. Clark, R. Condit, J. B. Blair, And M. Hofton. (2003). "Above-Ground Biomass Estimation in Closed Canopy Neotropical Forests Using Lidar Remote Sensing: Factors Affecting the Generality of Relationships." *Global Ecology and Biogeography* 12 (2): 147–159.

8. Fritz, A., T. Kattenborn, and B. Koch. "UAV-based photogrammetric point clouds—Tree stem mapping in open stands in comparison to terrestrial laser scanner point clouds." Int. Arch. Photogramm. Remote Sens. Spat. Inf. Sci 40 (2013): 141-146.

9. Goesele, Michael, Noah Snavely, Brian Curless, Hugues Hoppe, and Steven M. Seitz. "Multi-view stereo for community photo collections." In 2007 IEEE 11th International Conference on Computer Vision, IEEE, 2007. pp. 1-8.

10. Harwin, Steve, and Arko Lucieer. "Assessing the accuracy of georeferenced point clouds produced via multi-view stereopsis from unmanned aerial vehicle (UAV) imagery." Remote Sensing 4, no. 6 (2012): 1573-1599.

11. Horncastle, V. J., E. C. Hellgren, P. M. Mayer, A. C. Ganguli, D. M. Engle, And D. M. Leslie Jr. (2005) "Implications of Invasion by Juniperus Virginiana on Small Mammals in

The Southern Great Plains." *Journal of Mammalogy* 86 (6): 1144–1155.

12. Jensen, J. R. 2005. *Introductory Digital Image Processing: A Remote Sensing Perspective*. Upper Saddle River: Pearson Prentice Hall.

13. Lowe, David G. "Object recognition from local scale-invariant features." In Computer vision, 1999. The proceedings of the seventh IEEE international conference on, vol. 2, pp. 1150-1157. Ieee, 1999.

14. Lucas, R. M., N. Cronin, A. Lee, M. Moghaddam, C. Witte, and P. Tickle. (2006). "Empirical Relationships between AIRSAR Backscatter and Lidar-Derived Forest Biomass, Queensland, Australia." *Remote Sensing of Environment* 100 (3):407–425.

15. Norris, M., J. Blair, L. Johnson, and R. Mckane. (2001). "Assessing Changes in Biomass, Productivity, and C and N Stores Following Juniperus Virginiana Forest Expansion into Tallgrass Prairie" Canadian Journal of Forest Research 31: 1940–1946.

16. Owensby, C. E., K. R. Blan, B. J. Eaton, and O. G. Russ. 1973. "Evaluation of Eastern Redcedar Infestations in the Northern Kansas Flint Hills." *Journal of Range Management* 26 (4): 256–260. URL: http://www.jstor.org/stable/3896570.

17. Scharstein, D. and R Szeliski. (2002). "A Taxonomy and Evaluation of Dense Two-Frame Stereo Correspondence Algorithms". International journal of computer vision 47, no. 1-3 (2002): 7-42.

18. Slusher, J.P. (1995). "Wood Fuel for Heating." In University of Missouri Extension. URL: http://Extension.Missouri.Edu/Publications/Displaypub.Aspx?P=G5450

19. Snavely, Noah, Steven M. Seitz, and Richard Szeliski. "Skeletal graphs for efficient structure from motion." In CVPR, vol. 1, p. 2. 2008.

20. Starks, P. J., B. C. Venuto, J. A. Eckroat, and T. Lucas. (2011). "Measuring Eastern Red Cedar Juniperus Virginiana L. Mass with the Use of Satellite Imagery." *Rangeland Ecology & Management* 64 (2):178–186.

21. Stipe, D. J., and T. B. Bragg. (1989). "Effect of Eastern Red Cedar on Seedling Establishment of Prairie Plants." *Proceedings of the Eleventh North American Prairie Conference. 101–102*

22. Triggs, Bill, Philip F. McLauchlan, Richard I. Hartley, and Andrew W. Fitzgibbon. "Bundle adjustment—a modern synthesis." In *Vision algorithms: theory and practice*, pp. 298-372. Springer Berlin Heidelberg, 1999.

23. Wylie, B. K., D. J. Meyer, M. J. Choate, L. Vierling, P. K. Kozak, And R. O. Green. (2000). “Mapping Woody Vegetation and Eastern Red Cedar in The Nebraska Sand Hills Using AVIRIS.” Paper Read at AVIRIS Airborne Geoscience Workshop. JPL Publication 00-18. Pasadena, CA Jet Propulsion Laboratory, California Institute of Technology

24. Westoby, M. J., J. Brasington, N. F. Glasser, M. J. Hambrey, and J. M. Reynolds. "'Structure-from-Motion' photogrammetry: A low-cost, effective tool for geoscience applications." Geomorphology 179 (2012): 300-314.